

# Microbial communities demonstrate robustness in stressful environments due to predictable composition shifts

Jana S. Huisman<sup>1\*</sup>, Martina Dal Bello<sup>1,2,3</sup>, Jeff Gore<sup>1</sup>

<sup>1</sup> Physics of Living Systems, Massachusetts Institute of Technology, Cambridge, MA, United States of America

<sup>2</sup> Department of Ecology and Evolutionary Biology, Yale University, New Haven, CT 06511, USA

<sup>3</sup> Microbial Sciences Institute, Yale University, New Haven, CT 06511, USA

\*Correspondence: jhuisman@mit.edu (J.S. Huisman)

## Abstract

Environmental stress reduces species growth rates, but its impact on the function of microbial communities is less clear. Here, we experimentally demonstrate that increasing salinity stress shifts community composition towards species with higher growth rates. As a result, the mean community growth rate is more robust to increasing stress than the growth of individual species. We show this by propagating natural aquatic communities at multiple salinities and mapping the observed diversity onto the measured salinity performance curves of >80 bacterial isolates. We further validate these results with pairwise species competitions and in metagenomic data of natural communities sampled from estuarine environments. A Lotka-Volterra model including mortality and salinity-dependent growth rates recapitulates the observed robustness of community growth sustained by more abundant faster growers at high salinity. These results extend to other environmental stressors and point to fundamental mechanisms with which communities maintain growth despite deteriorating conditions.

# 1 Introduction

2 Microbial communities fulfill crucial ecosystem functions across soil, water and host-associated  
3 environments, from nutrient cycling to pathogen suppression [1, 2]. These functions are  
4 emergent, community-level properties resulting from the physiology of individual community  
5 members, their relative abundances, and the interactions between them [3]. Simple pertur-  
6 bations that affect individual species can have complex, nonlinear effects on the community.  
7 As a result, it remains unclear whether community-level properties are predictable in chang-  
8 ing environments. Specifically this raises the question how environmental stress – an abiotic  
9 change which reduces the growth of most species – impacts community composition and  
10 function.

11 Recent work has demonstrated that environmental changes can have predictable effects  
12 on community composition, although the functional consequences are less clear. Increasing  
13 temperature – which increases growth rates of most species – selects for communities  
14 dominated by slow growing species, both in controlled laboratory experiments with two or  
15 three species [4] and in marine microbial communities assayed with metagenomic data [5].  
16 At the same time, increased population-wide mortality (imposed through dilution) favors the  
17 faster growing species in pairwise competitions [6]. However, the impact of such composi-  
18 tional shifts on community function – and how this depends on the specific environmental  
19 change – remains unclear. An environmental stressor may impair community function as it  
20 reduces species growth rates, and the resulting shifts in the community composition could  
21 both amplify or buffer this effect.

22 Salinity is a key environmental stressor structuring microbial communities, particularly in soil  
23 and aquatic environments [7]. Climate change is expected to cause major disruption to ex-  
24 isting environmental salinity gradients. Sea-level rise, anthropogenic land use changes, and  
25 shifting precipitation patterns are increasing both the extent and variability of salt intrusion  
26 into freshwater systems [8, 9]. These salinity shifts can restructure microbial communities  
27 in complex ways: in salt marshes, for example, salinization reduces microbial methanogen-  
28 eisis and increases sulfur reduction [10]. Observations abound of community composition  
29 changing with salinity [7, 11, 12, 13, 14], yet we lack the ability to predict the strength and  
30 direction of this compositional shift and its functional consequences.

31 In contrast to the community-level ecological response, the mechanistic effects of salinity  
32 on individual bacteria are quite well understood. Salinity increases the osmolarity of the  
33 medium, causing water to flow out of bacterial cells and their turgor pressure to drop [15].  
34 This physiological stress reduces growth of most microbes [15]. The magnitude of this  
35 growth reduction is linked to species-specific mechanisms of osmoadaptation, which also  
36 determine the salinity at which a species achieves optimal growth. [15, 16]. While this  
37 optimal salinity is higher for salt-adapted (halotolerant or halophilic) bacteria than for other  
38 species, the mechanisms of stress beyond the optimal salinity are likely similar. However, a  
39 quantitative exploration of the relation between growth and salinity has remained restricted  
40 to common foodborne pathogens [17, 18], and little is known for environmental microbes.  
41 Moreover, the effects of salinity on community-level properties such as carrying capacity,  
42 competitive interactions, and overall growth remain largely unquantified.

43 Here, we ask to which extent community-level responses to increasing salinity can be pre-  
44 dicted from traits of the constituent species. We propagated natural communities at multiple  
45 salinities, and found that the mean community growth rate was remarkably robust to an  
46 increase in salinity despite decreasing growth rates for individual species. Combining mea-  
47 sured salinity performance curves – the maximum growth rate of a species as a function of

48 salinity – with a general model of bacterial competition under environmental stress, we could  
49 explain that the robustness of the community growth rate is the result of a shift in community  
50 composition towards species with high growth rates in stressful environments. We validated  
51 these predictions with pairwise competitions and metagenomic data of communities sam-  
52 pled across environmental salinity gradients. Since we predict that any environmental stres-  
53 sor that reduces the growth rate of most species will lead to these composition shifts and the  
54 associated robustness, this points towards fundamental mechanisms by which communities  
55 maintain function in stressful environments.

## 56 Results

### 57 **Community growth rates are robust due to compositional changes caused 58 by environmental stress**

59 To study how natural communities respond to increased environmental stress, we monitored  
60 the assembly of aquatic microbial communities at three different salinities (16, 31, 46 g/L sea  
61 salts), with fixed nutrient concentration and proportions of the five primary sea salts (NaCl,  
62 MgCl<sub>2</sub>, MgSO<sub>4</sub>, CaCl<sub>2</sub>, KCl). We sampled four aquatic microbial communities along a salinity  
63 gradient around the Boston harbor: the Charles River at the MIT sailing pavilion ("Brackish";  
64 4 g/L), the Boston harbor near the Institute for Contemporary Art ("Estuary"; 30 g/L), and the  
65 ocean at Canoe Beach, Nahant ("Marine 1 & 2"; 35 g/L; Fig. 1A). We serially propagated  
66 these communities *in vitro* every 2 days for a total of 7 cycles and assessed the diversity  
67 and composition of communities at 6 time points via 16S amplicon sequencing. After serial  
68 propagation, the communities reached a stable final composition (Fig. S1). Across the  
69 starting communities and propagation salinities, notably different steady state compositions  
70 were reached (Fig. S2). While the species richness and Shannon diversity decreased  
71 at higher salinity (Fig. 1D, S3), community biomass remained remarkably constant (Fig.  
72 S4). This raises the question whether we can predict changes in community composition in  
73 response to increasing salinity.

74 To understand the effects of salinity on the microbial community as a whole, we first charac-  
75 terized its effects on growth of the constituent species. We isolated 140 bacterial strains from  
76 the beginning and end of the serial dilution experiment, creating a library that includes > 60  
77 microbial species, across 31 genera and 17 families. This library spans the known diversity  
78 of marine bacteria (Table S1, Fig. S5). Supplementing this with eleven isolates previously  
79 obtained at our marine sampling location [19, 20], we covered on average  $95 \pm 6\%$  of the  
80 observed community diversity at the end of the serial dilution experiment (at 97% 16S iden-  
81 tity; Fig. S6). Maximizing phylogenetic diversity, we picked 85 isolates and measured their  
82 *salinity performance curve*, i.e. the effect of salinity (0-100 g/L sea salts) on maximum per  
83 capita growth rate (examples in Fig. 1B, all performance curves in Fig. S8). We find that  
84 isolates of the same family followed a similar salinity performance curve (Figs. 1C, S5, S8).  
85 The curves typically reach maximum growth rate  $r^{max}$  at an optimal salinity  $s^{opt}$  between  
86 0-35 g/L sea salts (ocean salinity is at 35 g/L), showing monotonically decreasing growth  
87 rates at salinities above this optimum (Fig. S8). Between 30 and 45 g/L, the growth rate of  
88 all isolates decreased by  $-0.06 \pm 0.01$  1/h on average. Carrying capacities were less strongly  
89 impacted by increasing salinity than the growth rates (Fig. S4).

90 Next, we asked how the growth rates of individual bacteria relate to the growth rate of the  
91 community. The community growth rate governs the community's recovery after perturba-  
92 tion and is intimately linked to community productivity, both crucial read-outs of community

function. To compute the mean *community growth rate* (CGR), we weighed the growth rate of a species at a particular salinity by its abundance in the community propagated at that salinity. While the individual species growth rates decreased above 30 g/L, we find no sign of decreasing CGR with increasing salinity (Fig. 1E). If anything, the CGR even increased for some communities at higher salinity. The CGR is thus more robust to increased environmental stress than the growth of individual species.

To test whether the robustness of the CGR can be explained by a shift in community composition, we computed a quantity that describes the relative abundance of fast growing species. To obtain this *community composition index* (CCI) we assigned each species a single value which describes its relative growth rate compared to other species, here the species max growth rate at 30 g/L  $r(30)$ , and computed the abundance weighted average of these species growth values for each community. We find that the CCI increases with increasing salinity for all starting communities (Fig. 1F). Increased environmental stress thus leads to a shift in species' relative abundances in favor of faster growing species, which confers robustness to the mean community growth rate.

## Stressful environments enrich for faster growing species

To explain the observed enrichment of faster growing species in stressful environments, we developed a Lotka-Volterra model describing the ecological dynamics of microbial communities. We assume that bacterial species  $N_i$  grow at a species and environment-specific growth rate  $r_i(s)$ , compete with each other with competition coefficients  $a_{ij}$ , and are removed from the environment at a rate  $\delta$ :  $\frac{dN_i}{dt} = r_i(s)N_i \cdot (1 - \sum_j a_{ij}N_j) - \delta N_i$  (Fig. 2A; Supplemental section S1). Continuous removal is common in natural environments, whether due to generalized predation or dilution [6, 5]. As a result of this mortality, the outcome of competition between two species depends on the removal rate  $\delta$  and the growth rates of both species [6, 4, 5] (Supplemental section S1). Environmental stress, which affects the growth rates of all species, will thus affect the outcome of interspecies competition.

Having measured the functional relationship between growth rate and salinity, we can simulate how community composition will change as the environment deteriorates. Our salinity performance curve measurements typically show a salinity  $s_i^{opt}$  at which the maximal growth rate  $r_i^{max}$  is reached, followed by an approximately linear decline in growth rate as salinity increases (here with slope  $b$ ), until growth reaches 0 at  $s_i^{max}$  (Figs. 1C, S8, S9). When simulating a 2-species community, we see that the relative abundance of the faster growing species increases with increasing salinity (Fig. 2B/C). Notably, this shift in community composition confers robustness to the *community growth rate* (CGR; black line in Fig. 2B). The CGR declines more slowly than the growth rate of the species that make up the community.

This robustness is recapitulated in more complex simulated communities ( $n = 50$ ), where the community growth rate increasingly approaches the salinity performance curves representing the fastest growing species (Fig. 2D). To describe the community composition index (CCI), we associate each species with its growth rate at 0 g/L salinity ( $r_i^{max}$ ) and compute the abundance weighted mean of these values for each of 50 simulated communities at a salinity  $s$ . Similar to the relative abundance of the faster grower in the 2-species case, the CCI increases with increasing salinity (red boxplots, Fig. 2E) and the corresponding CGR is more robust than the decline of the individual species growth rates (black boxplots and line, Fig. 2E). Importantly, this result only requires that the growth rate of all species declines with increasing salinity. We did not assume any effect of salinity on the interaction between

<sup>139</sup> species ( $\alpha_{ij}$ ). As such, the compositional shift towards fast growing species and the result-  
<sup>140</sup> ing robustness of the community growth rate are expected to hold for any environmental  
<sup>141</sup> stress that reduces the growth rate of most species.

<sup>142</sup> The enrichment of faster growing species at higher salinities and the associated robustness  
<sup>143</sup> of the CGR are not affected by model variations. Variation in the relative slopes of the salinity  
<sup>144</sup> performance curves between species leads to the same qualitative outcomes (Supplemental  
<sup>145</sup> section S1; Fig. S10). High removal rates  $\delta$  and increasing slopes increase the initial  
<sup>146</sup> strength of the CCI shift (Fig. S11, S12). They are made even more apparent in mixtures of  
<sup>147</sup> bacteria with different optimal salinities (Fig. S13).

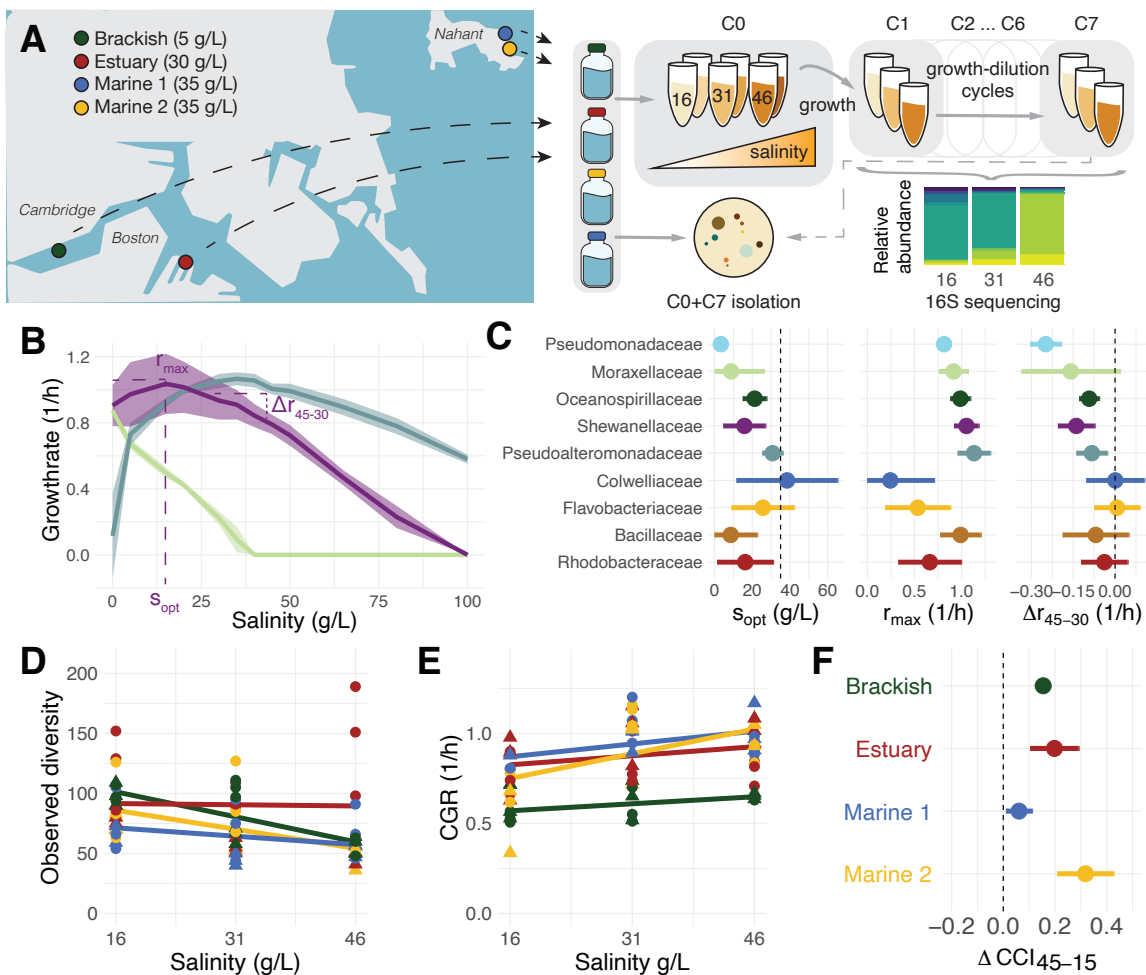


**Figure 1: The community growth rate of aquatic microbial communities is more robust to an increase in salinity than expected based on individual species growth rates, due to a shift in community composition towards faster growing species.** **A** Schematic overview of the serial dilution experiment: natural aquatic communities from four locations were propagated over 7 48-hour cycles (C1-C7) at 3 salinities. **B** Measured ‘salinity performance curves’ for three isolates (*Shewanella* in purple, *Acinetobacter* in light-green, *Pseudoalteromonas* in blue). The maximum growth rate (1/h) was extracted from 48hr OD600nm measurements at 12 salinities (n>3 replicates). **C** Optimal salinity ( $s_{opt}$ ), maximum growth rate ( $r_{max}$ ), and change in growth rate between 30 and 45 g/L ( $\Delta r_{45-30}$ ) for all families with at least 3 isolates. Drawn are mean  $\pm$  sd across n = 3 (Pseudomonadaceae) to n = 20 (Pseudoalteromonadaceae) isolates. In the case of  $s_{opt}$ , the vertical dashed line indicates ocean salinity at 35 g/L. **D** Richness (observed number of ASVs) of the propagated communities at the end of the experiment (C6, n = 3 at 15 °C and 20 °C, denoted by triangles and circles respectively). **E** Community growth rate (CGR) for communities at the end of the experiment (C6, n = 3 at 15 °C and 20 °C, denoted by triangles and circles respectively). **F** Change in the community composition index (CCI) between communities propagated at 15 g/L and 45 g/L (mean  $\pm$  se).

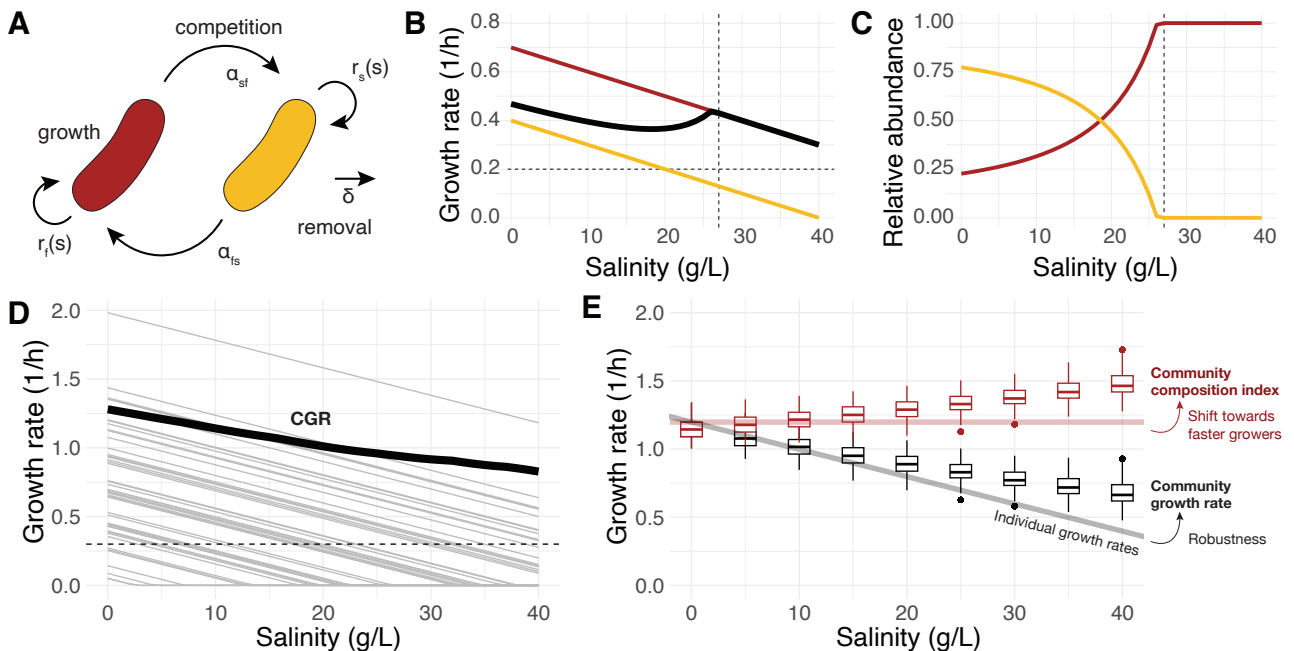


**Figure 2: Modeling predicts that an increase in salinity shifts community composition towards faster growing species and confers robustness to the community growth rate.** A) Model schematic of two species growing at rates  $r_{f/s}(s)$ , competing with inter-species interaction coefficients  $\alpha_{fs}, \alpha_{sf}$ , in the presence of removal from the environment at rate  $\delta$ . B) Growth rates of the two competing species are assumed to decline at the same rate ( $b = -0.02$ ; thin colored lines). The community growth rate (thick black line) declines more slowly. The dashed horizontal line indicates the strength of the removal rate ( $\delta = 0.2$ ). The dashed vertical line indicates the salinity at which the faster growing species first excludes the slower grower. C) Relative abundances of the two species at steady state at different salinities, with growth rates according to panel B. D) In a 50-species model where all growth rates decline at the same rate (thin grey lines), the community growth rate (thick black line) declines more slowly with increasing salinity. E) The robustness of the community growth rate is reproducible across 50 simulations of the 50-species communities (black boxplots). It is the result of a shift in community composition towards faster growing species (community composition index; red boxplots). If the community composition did not change with salinity (red line), the CGR would decline as the individual species growth rates (black line).

148 **Environmental stress can reverse pairwise competitive outcomes**

149 The model suggests that the outcome of pairwise bacterial competitions will change in a  
150 predictable way as a function of salinity. We set out to test whether an increase in salinity  
151 indeed favors faster growing bacteria *in vitro*, using 8 pairs of isolates from our library,  
152 competing at four salinities (16, 31, 46, 61 g/L; Fig. 3A). For each pairwise competition, we  
153 started three replicate pairs at three different starting ratios (95:5, 50:50, 5:95), and propa-  
154 gated them every second day for 7 cycles at four different salt concentrations (16, 31, 46,  
155 61 g/L). Across all conditions, the pairs reached stable final relative abundances (Fig. S14),  
156 with at least one salinity at which species coexisted at intermediate frequencies. The three  
157 different starting ratios led to similar final coexistence frequencies, revealing no evidence of  
158 bistability for any of the species pairs surveyed here.

159 We found that, in all 8 competitions tested, the faster growing strain had an increasing com-  
160 petitive advantage at higher salinity (Fig. 3F, S14), and community growth rate declined  
161 less rapidly than the individual species growth rates (Fig. 3G). For example, in the competi-  
162 tion between *Pseudoalteromonas arctica* (*Pa*) and *Shewanella xiamensis* (*Sx*) (Fig. 3B/C),  
163 the species coexisted at all salinities above 16 g/L, but the faster grower *Pa* became more  
164 abundant as salinity increases (Fig. 3B). As a result, the CGR stayed constant over a range  
165 of 30 g/L, while the growth rate of individual species declined, with *Sx*'s growth rate nearly  
166 halving across this range (Fig. 3C). This echos the findings of increasing CCI and robust  
167 CGR at higher salinity in our experiment with natural communities (Fig. 1), as predicted by  
168 our model (Fig. 2).

169 Strikingly, this dynamic is also observed in pairwise competitions where the slower growing  
170 species won at low salinities. When the same *Pa* was competed against an *Albirhodobac-  
171 ter sp.* (*Ar*), the latter won at low salinities (16 and 31 g/L) despite a substantial growth  
172 disadvantage (Fig. 3D/E). However, with increasing salinity (46 or 61 g/L) the faster grow-  
173 ing *Pa* took over the community (Fig. 3D). In this case the CGR was not just robust to  
174 increased environmental stress, but actually increased with increasing salinity (Fig. 3E).  
175 We therefore observed that a stress-induced shift in community composition towards faster  
176 growing species lends robustness to the mean community growth rate, both in laboratory  
177 experiments with complex natural communities and in well-controlled species pairs.

178 **Environmental communities are enriched in faster growing species at  
179 higher salinity**

180 Having gained insight into the effect of salinity on community dynamics *in vitro* and *in silico*,  
181 we next asked whether the increased abundance of faster growing species at high salinity  
182 can also be observed in natural microbial communities. In estuaries and inland seas, aquatic  
183 communities can be exposed to large seasonal or spatial salinity gradients. We identified  
184 four datasets of microbial communities sampled across such an environmental gradient: a  
185 3-year time series taken at the Pivers Island Coastal Observatory (PICO) [12], and spatial  
186 gradients in Chesapeake bay [13], the Baltic sea [11], and lagoons along the Beaufort sea  
187 coast [14] (Fig. 4A; Table S2).

188 Using genomic proxies to estimate the community composition index, we found an increas-  
189 ing proportion of species predicted to grow faster at higher salinity for all datasets (Fig. 4B).  
190 The 16S rRNA operon copy number is a genomic proxy for the maximum growth rate a  
191 bacterium can attain [21] (demonstrated for our isolate dataset in Fig. S15). By mapping  
192 each community member to its estimated copy number [22] and calculating the abundance

193 weighted mean copy number (MCN), we obtained a genomic proxy for the CCI [5]. We  
194 found that the MCN significantly increased as a function of salinity for the Baltic sea, Beau-  
195 fort sea, and Pivers island datasets. While not significant, Chesapeake bay also showed  
196 an increasing MCN with increasing salinity. This increase continued to be highly significant  
197 when accounting for all other environmental predictors measured in these datasets (Fig.  
198 4B). Of the other predictors, increasing temperature significantly reduced MCN in the Baltic  
199 sea and Chesapeake bay datasets. This has previously been described for other datasets  
200 of marine microbial communities and is consistent with our modeling framework, given tem-  
201 perature's known role in increasing bacterial growth rates [5, 4]. To conclude, the community  
202 shift towards faster growing species at high salinity that we observed *in vitro* is recapitulated  
203 in environmental datasets despite differences in temperature and nutrient availability.

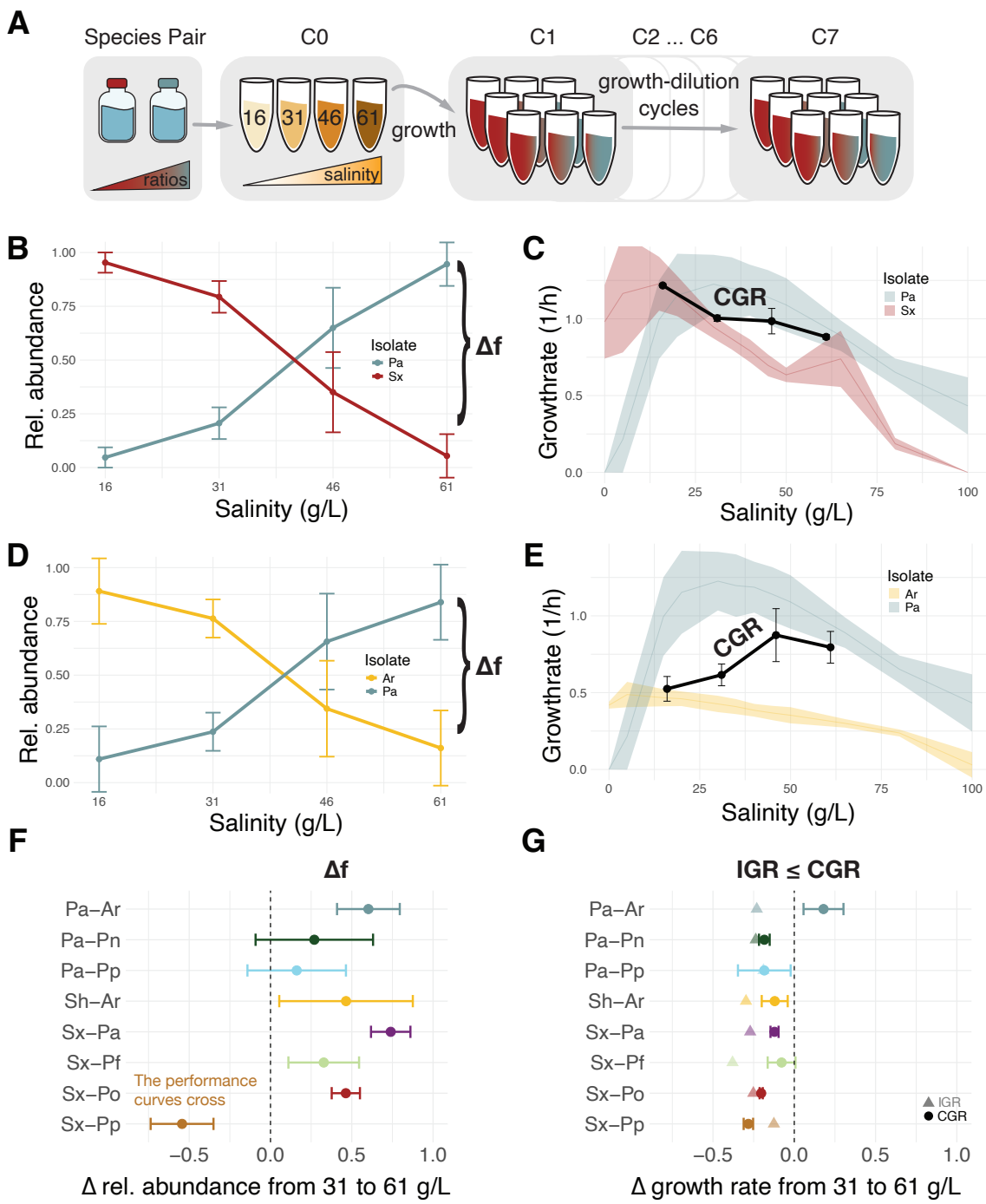


**Figure 3: In pairwise co-culture, higher salinity favors the faster growing species.**

**A)** Experimental overview: we mixed three replicates of two species at three ratios (95:5, 50:50, 5:95) and propagated them at 4 salinities (16, 31, 46, 61 g/L) for 14 days (C1-C7).

**B)** Relative abundance of *Pseudoalteromonas arctica* (blue; Pa) and *Shewanella xiamensis* (red; Sx) after propagation at 4 salinities (mean and sd across three biological replicates at three different initial ratios). **C**) Salinity performance curves for Pa and Sx (ribbons show mean  $\pm$  sd across  $n \geq 3$  replicates). The black line indicates the CGR of the pairs after 14 days of propagation at 16, 31, 46, 61 g/L salinity. **D, E)** As panel B, C but for the competition between *Pseudoalteromonas arctica* (blue; Pa) and *Albirrhodobacter sp.* (yellow; Ar). **F)** The difference in the relative abundance of the faster growing species upon propagation at 31 and 61 g/L, across 8 species pairs. **G)** The difference in the community growth rate (CGR, circles) and mean isolate growth rate (IGR, triangles) upon propagation at 31 and 61 g/L, across 8 species pairs.

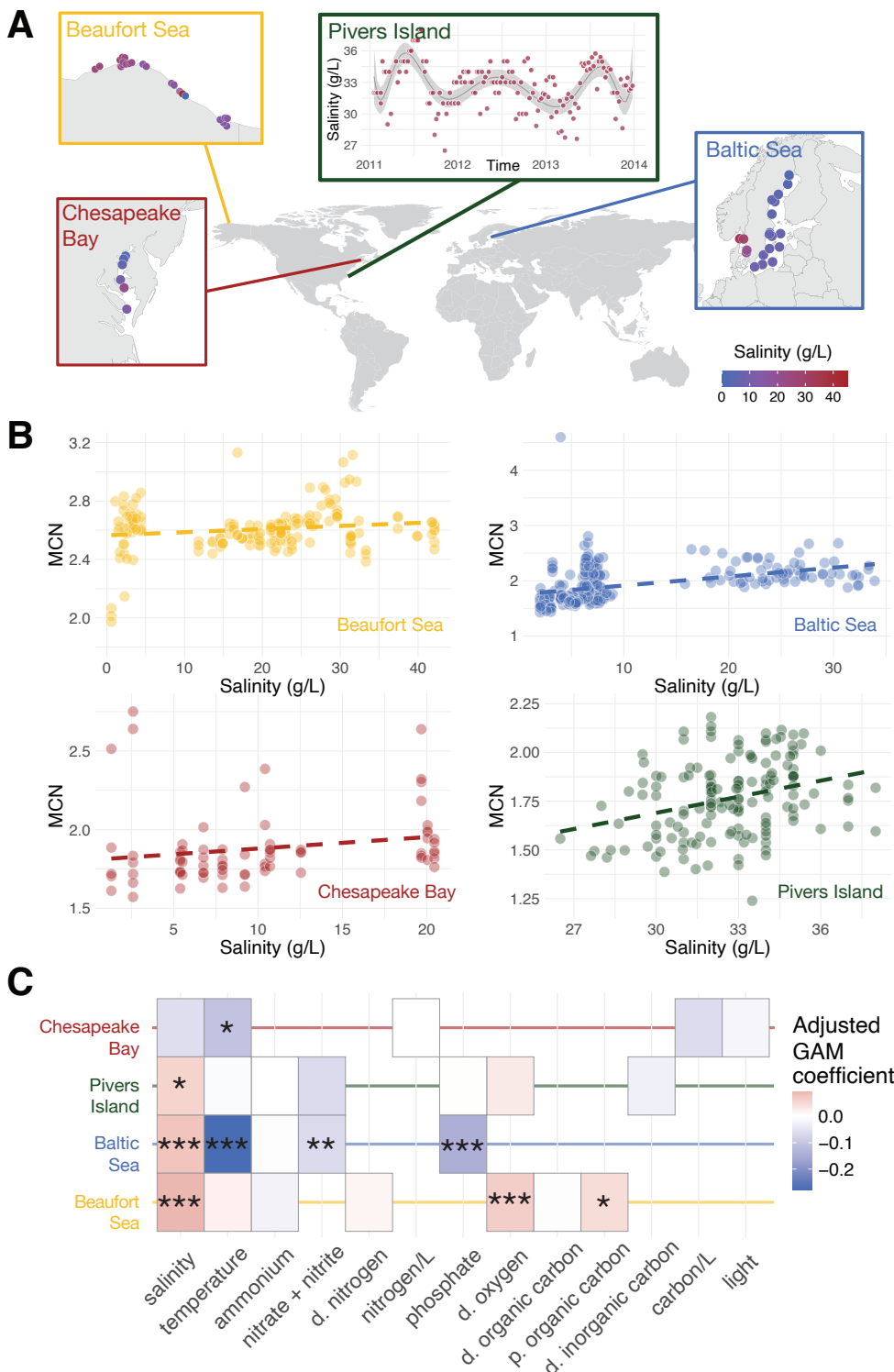


**Figure 4: Higher salinity favors faster growers in natural estuarine communities, despite temperature and nutrient differences.** A) Map indicating the sampling locations of the four datasets: Beaufort sea, Pivers island, Chesapeake bay, and the Baltic sea. B) Mean copy number of the 16S rRNA gene (MCN) of each community sampled in the different datasets, plotted as a function of salinity at the location and time of sampling. C) Coefficient of variance explained by different predictors of mean copy number. The color corresponds to the estimated parametric coefficient in the model, multiplied by the standard deviation of the environmental predictor. Environmental predictors were abbreviated with "p." for particulate, and "d." for dissolved. The asterisks indicate significance at \*\*\* $p < 0.001$ , \*\* $p < 0.01$ , \* $p < 0.05$ .

204 **Discussion**

205 In this work, we set out to investigate how environmental stress impacts community com-  
206 position and function. We showed that microbial community growth rate – which sets the  
207 pace for fundamental ecosystem functions, including biomass production and the ability to  
208 recover from perturbations – is remarkably robust to environmental stresses that reduce  
209 species' growth rates. This robustness is the result of a change in community composi-  
210 tion towards faster growing species. We have demonstrated this in the context of natural  
211 aquatic communities propagated at different salinities, as well as pairwise competitions and  
212 environmental estuarine datasets.

213 This compositional shift and community robustness likely extends beyond salinity to other  
214 stressors, including pH, temperature and chemical pollutants. Our modeling framework  
215 lacks environment- or stressor-specific assumptions and would make similar predictions  
216 for any stressor that reduces the growth of most bacteria. Indeed, prior research noted that  
217 growth of a mixed community of bacteria proved more robust to the influence of chemical pol-  
218 lutants than growth of the constituent members [23]. In pairwise competitions, faster growth  
219 proved the most important determinant to predict competitive outcomes in the presence of  
220 increasing sublethal concentrations of antibiotics [24], increasing daily dilution rates [6], and  
221 reduced temperature [4]. For temperature this effect was also observed in environmental  
222 datasets, where a decrease in temperature corresponds to a decrease in the growth rate of  
223 species and leads to the same community shift as an increase in salinity [5]. All these obser-  
224 vations would be consistent with emergent robustness of the community growth rate due to  
225 a compositional shift towards faster growers in the presence of environmental stress.

226 Environmental stress is often characterized by changes in not only one, but multiple envi-  
227 ronmental variables. Here, we found that the impact of salinity on the composition of natural  
228 communities was robust to environmental confounders such as temperature and nutrient  
229 concentrations. However, interactions between changing variables may still structure bac-  
230 terial growth in non-trivial ways. For instance, higher temperatures can expand the range  
231 of salinity tolerance for some species ([25] and own preliminary data). More growth mea-  
232 surements are needed to parametrize performance functions across multiple simultaneously  
233 varying variables, and to assess the predictability of community-level behavior under multi-  
234 variate stressors.

235 Importantly, while environmental stress did not affect community growth, it did lower commu-  
236 nity diversity. This highlights a dilemma in how to assess ecosystem health and functioning:  
237 high community biomass and growth rates might be achieved even when the community  
238 diversity is already severely impacted. The loss of genetic diversity at both within- and be-  
239 tween species levels is irreversible without influx from the external species pool and may  
240 lead the community to enter a long-term alternative stable state. The loss of functional  
241 diversity can also reduce resilience to future perturbations with a different stressor. This  
242 underlines the importance of assessing diversity also in the case of communities whose  
243 biomass production and/or growth rate seems robust to stress.

244 To conclude, we have uncovered a general principle governing the response of communi-  
245 ties to environmental stress. Increasing stress causes the community composition to shift  
246 towards faster growing species, which confers robustness to the mean community growth  
247 rate.

248 **Methods**

249 **Sampling and C0 species isolation**

250 We sampled water at three locations around Boston on March 31st 2023. The locations  
251 span a natural salinity gradient: The Charles River at the MIT sailing pavilion ("Brackish";  
252 4 g/L; 10 °C), the Boston harbor near the Institute for Contemporary Art ("Estuary"; 30 g/L;  
253 6 °C), and the ocean at Canoe Beach, Nahant ("Marine 1"; 35 g/L; 7 °C). Temperature and  
254 salinity were recorded at the time of sampling (refractometer kindly borrowed from the Fakhri  
255 lab, MIT). Per location, we filtered 2L of water using a 63  $\mu\text{m}$  filter (kindly borrowed from  
256 the Cordero lab, MIT; filter pre-washed with water from the respective location) to remove  
257 particulate matter and larger eukaryotic cells. We concentrated the samples by centrifuging  
258 them at 4000 rpm for 5 minutes and keeping only the bottom 10% of the sample. This  
259 resulted in 100 mL of concentrated water per inoculum sample.

260 We additionally sampled brown macroalgae (likely *Ascophyllum nodosum*) at Nahant. To  
261 obtain the algae-attached communities, we placed seaweed blades into 8 50 mL conical  
262 tubes (Falcon) and vortexed them in seawater from Nahant for 2 minutes prior to sieving  
263 with the 63  $\mu\text{m}$  filter. The 8 tubes were centrifuged at 4000 rpm for 5 minutes, we combined  
264 the bottom 10% (40 mL) into a single falcon tube. The resulting concentrated water was  
265 used as fourth aquatic community sample ('Marine 2').

266 The majority of the sample was used to inoculate a serial dilution experiment (described  
267 below). The rest was frozen both directly and with 30% glycerol at -80 °C. To isolate species  
268 from the original communities, we plated 150  $\mu\text{L}$  concentrated inoculum onto 2 replicate  
269 20% marine broth agar plates (MB; Becton Dickinson; bacteriological agar VWR). These  
270 were left to grow at room temperature for 3 days. Then, we visually inspected the plates,  
271 picked colonies, and streaked them out individually ('C0 isolates'). We revisited plates after  
272 7 days, and picked 8 additional colonies in the same manner. For permanent storage, we  
273 used the streaked plates to pick one colony per isolate and transferred it into a 1mL deepwell  
274 plate (Eppendorf) with 400  $\mu\text{L}$  MB. After 2 days of growth at room temperature on a shaker  
275 at 1350 rpm, we added 400  $\mu\text{L}$  of sterilized 50/50 glycerol to each well, and transferred the  
276 plates to the -80 °C freezer.

277 **Serial dilution experiment and C7 species isolation**

278 To obtain stable communities at different salt conditions, we ran a 14-day serial dilution  
279 experiment in which the 4 inocula were adapted to 3 different salt concentrations (16, 31,  
280 46 g/L sea salts). We used undiluted marine broth (MB, Becton Dickinson) as base medium  
281 (37 g/L MB corresponds to 31 g/L sea salts). With 'sea salts' we denote the 5 primary  
282 salts present in MB, at their respective relative proportions: 19.45 g/L Sodium Chloride, 5.9  
283 g/L Magnesium Chloride, 3.24 g/L Magnesium Sulfate, 1.8 g/L Calcium Chloride, 0.55 g/L  
284 Potassium Chloride. To obtain the other salt concentrations, the amount of nutrients was  
285 kept fixed: the lower salinity (16 g/L) was reached by diluting the MB and adding nutrients  
286 (peptone, yeast, ferric citrate), and the higher salinity (46 g/L) by supplementing MB with  
287 sea salts. All three concentrations of MB were filter sterilized by passing through a .2  $\mu\text{m}$   
288 filter (Stericup, Millipore) and stored in the dark at 4 °C.

289 To start the experiment, we inoculated 3 replicates of each aquatic sample (10  $\mu\text{L}$  concen-  
290 trated inoculum) into a 96 well 500  $\mu\text{L}$  deepwell plate (Eppendorf) with 290  $\mu\text{L}$  MB per well,  
291 at 3 different salt concentrations (16, 31, 46 g/L sea salts). This yielded a total of 9 inocu-

292 lated communities for each of the 4 samples, the remaining 60 wells were used as spacing  
293 and blanks to control for contamination. We incubated two separate plates at 15 and 20 °C.  
294 Plates were kept on benchtop shakers (Titramax 100) operated at 1200 rpm. Every second  
295 day for 2 weeks, we diluted the culture in each well 1:30 and transferred the communities  
296 to a plate with fresh culture medium (using the Integra VIAFLO96). After every transfer, we  
297 used 100 µL from the old plate to measure pH (Thermo Fisher Orion Star A211) and OD600  
298 (Tecan Infinite M Nano). The remainder of the old plate (190 µL per well) was then stored at  
299 -80 °C, to be used for DNA extraction.

300 After 7 dilution cycles (14 days; the end of the experiment), we diluted each community  $10^{-7}$   
301 in PBS. We plated 50 µL onto 150x15 mm petri dishes with 20% marine broth agar (MB;  
302 Becton Dickinson; bacteriological agar VWR). The three replicates of the Marine 1 inoculum  
303 at 16 g/L salt at 15 °C and 20 °C were additionally plated at a dilution of  $10^{-5}$ . We counted  
304 all colonies on these plates, picked representative colonies displaying different morphology,  
305 and individually streaked them onto 100x15 mm 20% MB agar plates ('C7 isolates'). Single  
306 isolates were picked from these plates, grown in 1 mL MB overnight, combined with 0.5  
307 mL sterile glycerol and stored at -80 °C. Additionally, at dilution cycle 7, we transferred the  
308 deepwell plates one more time to allow for long-term storage of the full communities. After  
309 pH and OD600 measurement on day 16, we added 200 µL 50/50 glycerol to these cycle 8  
310 plates and stored them at -80 °C.

### 311 Isolate 16S rRNA sequencing and species identification

312 C0 and C7 isolates were streaked onto fresh 20% MB agar plates from the -80 °C stock  
313 and sent for 16S rRNA gene Sanger sequencing with Azenta Life Sciences. We used their  
314 in-house pipeline to trim and merge the forward and reverse reads. We assigned taxonomy  
315 using DADA2 [26] and the SILVA database (v138.1) [27].

316 We aligned the 16S genes with MAFFT [28], and used RaxML [29] with a GTR model with  
317 Γ site variation to estimate a maximum likelihood phylogeny for all isolates.

### 318 Community 16S rRNA sequencing and ASV calling

319 To obtain community 16S sequencing data, we sent each replicate community from the C1,  
320 C3, C5, C6, C7 cycles, as well as two replicates per C0 inoculum for sequencing (Novo-  
321 gene). We used v4-v5 primers to obtain 250bp paired-end reads on an Illumina NovoSeq  
322 6000. In total, we sequenced 368 communities.

323 We used the DADA2 [26] pipeline to trim and filter the sequencing reads, infer amplicon  
324 sequence variants (ASVs), merge paired reads, and remove chimeras. We additionally used  
325 it to assign species taxonomy according to the SILVA database (v138.1) [27]. For further  
326 analyses we removed spurious ASVs that were classified as mitochondria or non-bacterial,  
327 and ASVs that were only found in a single sample.

328 We calculated the species richness by counting the number of different ASVs in a sample.  
329 We use rrnDB to assign each ASV a copy number. We assigned each ASV a copy number  
330 according to the lowest taxonomic rank for which a value was available in the database.  
331 Using these copy numbers, we calculated the true relative abundance of each ASV. For each  
332 sample we additionally calculated the mean copy number (MCN) which denotes the average  
333 copy number of the ASVs in the sample (weighted by their relative abundance).

334 Four samples from C7 showed unexpectedly high diversity. These were all co-located with

335 C0 samples in the first two rows of one of the plates sent for sequencing, which leads us  
336 to believe there was a contamination during transport or sample handling. As a result, we  
337 used C6 for subsequent analysis.

338 ASVs were matched to isolate 16S rRNA gene sequences using BLAST at > 97% iden-  
339 tity [30].

### 340 Growth rates

341 To measure the growth of different aquatic isolates across a gradient of salinity, we used  
342 12 different media with the nutrients of normal MB (except Sodium Fluoride) and varying  
343 amounts of the 5 primary sea salts (NaCl, MgCl, MgSO, CaCl, KCl) in the same ratio as  
344 in MB. A MB- nutrient only solution was combined with MB with 100 g/L salts in different  
345 ratios to obtain 0, 5, 15, 20, 30, 35, 40, 45, 50, 65, 80, 100 g/L MB solutions. The two  
346 stock solutions were filter sterilized by passing through a .2  $\mu$ m filter (Stericup, Millipore)  
347 and stored in the dark at 4°C.

348 Strains were streaked from -80 °C stocks onto 20% MB agar, grown at room temperature for  
349 2-4 days and stored at 4 °C. For each strain, we picked a replicate isolate on three separate  
350 days, and grew it in 3 mL MB in a 17x100 mm culture tube (VWR) for 48 hrs at 20 °C with  
351 spinning ( $\sim 100\pm25$  rpm) on a rotary lab suspension mixer (TMO-1700, MRC Lab).

352 We diluted these overnight cultures 100-fold in MB, and used them to inoculate a 96 well  
353 plate (hereafter called the ‘measurement plate’). We added 2  $\mu$ L diluted isolate culture to  
354 wells containing 200  $\mu$ L MB at 12 different salinities. The sides were taped against evapora-  
355 tion. Growth rates were measured on a Tecan Infinite M Nano, for 48 hours at 20 °C.

356 We used the R package *gcplyr* (v1.11.0) [31] to estimate growth rates from the OD mea-  
357 surements. Specifically, we smoothed the measured OD across 21 minutes (7 datapoints;  
358 sliding window) and used *gcplyr* to estimate the derivative of the log OD curve. This deriva-  
359 tive corresponds to the average growth rate across a 1-hr window. We denote the maximum  
360 growth rate for growth at this salinity  $r_{max}$ . To exclude spurious results, we did not assess  
361 the derivative in the first 3 hours of growth and if the OD for a given strain at a given salinity  
362 did not exceed 0.1, we set  $r_{max} = 0$ .

363 We used the package *segmented* in R, to fit both a linear and a piecewise linear function  
364 with two segments to the measured salinity performance curves. If the adjusted R squared  
365 of the linear fit was better than that of the 2-segment model, the linear fit was kept and  $s^{opt}$   
366 assumed to be 0. The latter ( $s^{opt} = 0$ ) was also assumed if the 2-segment model inferred  
367 a negative slope for the first segment. In all other cases,  $s^{opt}$  was assumed to be at the  
368 inferred breakpoint of the two segments.

### 369 Pairwise Competitions

370 Using the C0 and C7 isolates, we selected 8 strains for pairwise competitions (Pseudoal-  
371 teromonas arctica *Pa*, Shewanella xiamensis *Sx*, Shewanella sp. *Sh*, Albirhodobacter sp.  
372 *Ar*, Pseudoalteromonas ostrae *Po*, Pseudoalteromonas nitrificiens *Pn*, Pseudomonas fragi  
373 *Pf*, and Psychrobacter piscatorii *Pp*). The isolates were selected based on 16S similarity to  
374 dominant ASVs at the end of the serial dilution experiment, discernible phenotypes on MB  
375 agar plates, and different salinity performance curves.

376 To reach the steady state outcome of the competition, we propagated the 8 pairs for 14 days

377 at 4 different salt concentrations (16, 31, 46, 61 g/L sea salts) and 3 different starting ratios  
378 (95:5, 50:50, 5:95). The media was prepared as for the growth rate measurements.

379 To start the experiment, we grew 3 biological replicates of all 8 strains in MB for 48 hours,  
380 washed them twice in PBS, OD standardized to the lowest OD, mixed strains in correspon-  
381 dence with the intended starting ratio, and inoculated 10  $\mu$ L of this strain mixture into four  
382 (one per salinity) 96 well 500  $\mu$ L deepwell plates (Eppendorf) with 290  $\mu$ L growth medium  
383 per well. Monoculture growth controls were included for each biological replicate. Unfortu-  
384 nately the control for isolate 6 was contaminated (50-50) by isolate 8 during inoculation, and  
385 not used for further analysis. The four plates were incubated at room temperature (20-21  
386 °C) on a benchtop shaker (Titramax 100). Every second day, we diluted the culture in each  
387 well 1:30 and transferred the communities to a plate with fresh culture medium (using the  
388 Integra VIAFLO96). After every transfer, we used 100  $\mu$ L from the old plate to measure  
389 OD600 (Tecan Infinite M Nano).

390 At the start of the experiment and after cycles C1, C3, C5, C6, C7, we diluted each plate  
391  $10^{-6}$  and  $10^{-7}$  in PBS, spot-plated 10  $\mu$ L per well, and counted the corresponding colonies  
392 after 2-3 days. For pairs *Pa-Sx*, *Sx-Pp*, *Sx-Pf*, *Sx-Po*, *Pa-Pp*, and *Pa-Pn* we used the counts  
393 at  $10^{-6}$  for further analysis. For the two pairs with *Ar*, i.e. *Pa-Ar* and *Sh-Ar*, we used dilution  
394  $10^{-7}$ .

## 395 Modeling

396 We describe our modeling framework in more detail in Supplementary Section S1. In brief,  
397 we used a generalized Lotka-Volterra model with constant dilution rate  $\delta$  to model the com-  
398 petition between two or more species,  $N_i$ :

$$\frac{dN_i}{dt} = r_i(s)N_i \cdot (1 - \sum_{j \in 1 \dots M} a_{ij}N_j) - \delta N_i. \quad (1)$$

399 Here  $r_i(s)$  denotes the growth rate at salinity  $s$ . The self-inhibition terms are all set to  $a_{ii} = 1$   
400 (equivalent to normalizing by carrying capacity), and the terms  $a_{ij}$  describe the effect of  
401 species  $N_j$  on the growth of  $N_i$ .

402 We simulated these equations deterministically using the R programming language [32].  
403 Growth rates  $r$  were sampled from a normal distribution  $\mathcal{N}(0.7, 0.2)$ ,  $a_{ii} = 1$ , and  $a_{ij}$  were  
404 sampled from a uniform distribution on the interval  $(0, 2\alpha)$ . The mean interaction strength is  
405  $\alpha = 0.25$  for the main-text figures.

406 To study the effect of changing salinity, three different scenarios were assumed for  $r_i(s)$ : a  
407 parallel decline where  $r_i^{max}$  is sampled but the slope is fixed for all species, a converging  
408 decline where  $r_i^{max}$  is sampled and  $s^{max}$  is fixed for all species, and a diverging decline  
409 where  $r^{max}$  is fixed for all species but the slope is sampled (Supp. Fig. S10A).

## 410 Environmental metagenomic samples

411 We searched Pubmed for published research papers that sampled aquatic microbial com-  
412 munities at different salinities and reported the 16S sequencing data. We added articles that  
413 were identified via independent routes or from forward/back citations of articles previously  
414 identified. By screening abstracts for relevance, we narrowed several hundreds of papers  
415 down to a set of roughly 20 articles, for which we read the full text to determine their suitabil-  
416 ity for inclusion in our comparison. Articles were excluded if they had a salinity range  $< 10$

417 g/L, involved non-aquatic systems, contained < 20 data points, contained no information  
418 on confounding environmental variables such as temperature, or if the 16S data was not  
419 available.

420 For the resulting studies [12, 11, 13, 14] we downloaded 16S sequencing data, metadata,  
421 and all measured environmental variables (Table S2). For two of these [13, 14] only raw  
422 reads were available, which required pre-processing with DADA2 to obtain the table of ASV  
423 abundances. We followed the same steps as detailed in methods section "Community 16S  
424 rRNA sequencing", with trimming parameters optimized to each dataset.

425 We fitted general additive models to our data, taking into account all measured environmen-  
426 tal variables for each dataset (provided they were not highly correlated with other included  
427 variables).

## 428 **Data availability**

429 All code and data is available at: <https://github.com/JSHuisman/salinity>.

## 430 **Acknowledgements**

431 The authors thank Shreyansh Umale and other members of the Gore lab for helpful discus-  
432 sions about this work. JSH was supported by Human Frontier Science Program (HFSP)  
433 Postdoctoral Fellowship LT0045/2023-L.

## 434 **Author contributions**

435 JSH designed the study; performed sampling, in vitro experiments (serial dilution, growth  
436 and pairwise competition) and modeling; contributed to the environmental data analysis;  
437 visualized results; and wrote the first draft of the manuscript. MDB designed the study; per-  
438 formed sampling and environmental data analysis; contributed to serial dilution experiments  
439 and data visualization; and edited the manuscript. JG designed the study; supervised in  
440 vitro experiments and modeling; and edited the manuscript.

# 1 References

- [1] Naomi M Levine, Harriet Alexander, Erin M Bertrand, Victoria J Coles, Stephanie Dutkiewicz, Suzana G Leles, and Emily J Zakem. Microbial ecology to ocean carbon cycling: from genomes to numerical models. *Annual Review of Earth and Planetary Sciences*, 53, 2025.
- [2] Frances Spragge, Erik Bakkeren, Martin T Jahn, Elizete BN Araujo, Claire F Pearson, Xuedan Wang, Louise Pankhurst, Olivier Cunrath, and Kevin R Foster. Microbiome diversity protects against pathogens by nutrient blocking. *Science*, 382(6676):eadj3502, 2023.
- [3] Joshua E Goldford, Nanxi Lu, Djordje Bajic, Sylvie Estrela, Mikhail Tikhonov, Alicia Sanchez-Gorostiaga, Daniel Segre, Pankaj Mehta, and Alvaro Sanchez. Emergent simplicity in microbial community assembly. *Science*, 361(6401):469–474, 2018.
- [4] Simon Lax, Clare I. Abreu, and Jeff Gore. Higher temperatures generically favour slower-growing bacterial species in multispecies communities. *Nature Ecology and Evolution*, 4:560–567, 4 2020.
- [5] Clare I. Abreu, Martina Dal Bello, Carina Bunse, Jarone Pinhassi, and Jeff Gore. Warmer temperatures favor slower-growing bacteria in natural marine communities. *Science Advances*, 9, 2023.
- [6] Clare I. Abreu, Jonathan Friedman, Vilhelm L. Andersen Woltz, and Jeff Gore. Mortality causes universal changes in microbial community composition. *Nature Communications*, 10, 12 2019.
- [7] Catherine A Lozupone and Rob Knight. Global patterns in bacterial diversity, 2007.
- [8] A. Smajgl, T. Q. Toan, D. K. Nhan, J. Ward, N. H. Trung, L. Q. Tri, V. P.D. Tri, and P. T. Vu. Responding to rising sea levels in the mekong delta. *Nature Climate Change*, 5:167–174, 1 2015.
- [9] Lijing Cheng, Kevin E. Trenberth, Nicolas Gruber, John P. Abraham, John T. Fasullo, Guancheng Li, Michael E. Mann, Xuanming Zhao, and Jiang Zhu. Improved estimates of changes in upper ocean salinity and the hydrological cycle. *Journal of Climate*, 33:10357–10381, 12 2020.
- [10] Jun Zhao, Seemanti Chakrabarti, Randolph Chambers, Pamela Weisenhorn, Rafael Travieso, Sandro Stumpf, Emily Standen, Henry Briceno, Tiffany Troxler, Evelyn Gaiser, John Kominoski, Braham Dhillon, and Willm Martens-Habbena. Year-around survey and manipulation experiments reveal differential sensitivities of soil prokaryotic and fungal communities to saltwater intrusion in florida everglades wetlands. *Science of The Total Environment*, 858:159865, 2 2023.
- [11] Meike AC Latz, Agneta Andersson, Sonia Brugel, Mikael Hedblom, Krzysztof T Jurdzinski, Bengt Karlsson, Markus Lindh, Jenny Lycken, Anders Torstensson, and Anders F Andersson. A comprehensive dataset on spatiotemporal variation of microbial plankton communities in the baltic sea. *Scientific Data*, 11(1):18, 2024.
- [12] Christopher S Ward, Cheuk-Man Yung, Katherine M Davis, Sara K Blinebry, Tiffany C Williams, Zackary I Johnson, and Dana E Hunt. Annual community patterns are driven by seasonal switching between closely related marine bacteria. *The ISME journal*, 11(6):1412–1422, 2017.
- [13] Jacob A Cram, Ashley Hollins, Alexandra J McCarty, Grace Martinez, Minning Cui, Maya L Gomes, and Clara A Fuchsman. Microbial diversity and abundance vary along salinity, oxygen, and particle size gradients in the chesapeake bay. *Environmental Microbiology*, 26(1):e16557, 2024.
- [14] Colleen TE Kellogg, James W McClelland, Kenneth H Dunton, and Byron C Crump. Strong seasonality in arctic estuarine microbial food webs. *Frontiers in Microbiology*, 10:2628, 2019.

- [15] Erhard Bremer and Reinhard Krämer. Responses of microorganisms to osmotic stress. *Annu. Rev. Microbiol*, 73:313–334, 2019.
- [16] Krzysztof T Jurdzinski, Maliheh Mehrshad, Luis Fernando Delgado, Ziling Deng, Stefan Bertilsson, and Anders F Andersson. Large-scale phylogenomics of aquatic bacteria reveal molecular mechanisms for adaptation to salinity. *Science advances*, 9(21):eadg2059, 2023.
- [17] T. A. McMeekin, R. E. Chandler, P. E. Doe, C. D. Garland, June Olley, S. Putro, and D. A. Ratkowsky. Model for combined effect of temperature and salt concentration/water activity on the growth rate of *staphylococcus xylosus*. *Journal of Applied Bacteriology*, 62:543–550, 6 1987.
- [18] David W Miles, Thomas Ross, June Olley, and Thomas A McMeekin. Development and evaluation of a predictive model for the effect of temperature and water activity on the growth rate of *vibrio parahaemolyticus*. *International Journal of Food Microbiology*, 38:133–142, 9 1997.
- [19] Tim N Enke, Manoshi S Datta, Julia Schwartzman, Nathan Cermak, Désirée Schmitz, Julien Barrere, Alberto Pascual-García, and Otto X Cordero. Modular assembly of polysaccharide-degrading marine microbial communities. *Current Biology*, 29(9):1528–1535, 2019.
- [20] Matti Gralka, Shaul Pollak, and Otto X Cordero. Genome content predicts the carbon catabolic preferences of heterotrophic bacteria. *Nature Microbiology*, 8(10):1799–1808, 2023.
- [21] Benjamin RK Roller, Steven F Stoddard, and Thomas M Schmidt. Exploiting rrna operon copy number to investigate bacterial reproductive strategies. *Nature microbiology*, 1(11):1–7, 2016.
- [22] Steven F Stoddard, Byron J Smith, Robert Hein, Benjamin RK Roller, and Thomas M Schmidt. rrn db: improved tools for interpreting rrna gene abundance in bacteria and archaea and a new foundation for future development. *Nucleic acids research*, 43(D1):D593–D598, 2015.
- [23] Thomas P Smith, Tom Clegg, Emma Ransome, Thomas Martin-Lilley, James Rosindell, Guy Woodward, Samraat Pawar, and Thomas Bell. High-throughput characterization of bacterial responses to complex mixtures of chemical pollutants. *Nature Microbiology*, 9(4):938–948, 2024.
- [24] Daniel R Amor and Jeff Gore. Fast growth can counteract antibiotic susceptibility in shaping microbial community resilience to antibiotics. *Proceedings of the National Academy of Sciences*, 119(15):e2116954119, 2022.
- [25] Antonio Ventosa, Joaquín J Nieto, and Aharon Oren. Biology of moderately halophilic aerobic bacteria. *Microbiology and molecular biology reviews*, 62(2):504–544, 1998.
- [26] Benjamin J. Callahan, Paul J. McMurdie, Michael J. Rosen, Andrew W. Han, Amy Jo A. Johnson, and Susan P. Holmes. Dada2: High-resolution sample inference from illumina amplicon data. *Nature Methods*, 13:581–583, 6 2016.
- [27] Christian Quast, Elmar Pruesse, Pelin Yilmaz, Jan Gerken, Timmy Schweer, Pablo Yarza, Jörg Peplies, and Frank Oliver Glöckner. The silva ribosomal rna gene database project: Improved data processing and web-based tools. *Nucleic Acids Research*, 41, 1 2013.
- [28] Kazutaka Katoh and Daron M Standley. Mafft multiple sequence alignment software version 7: improvements in performance and usability. *Molecular biology and evolution*, 30(4):772–780, 2013.
- [29] Alexandros Stamatakis. Raxml version 8: a tool for phylogenetic analysis and post-analysis of large phylogenies. *Bioinformatics*, 30(9):1312–1313, 2014.
- [30] Stephen F. Altschul, Warren Gish, Webb Miller, Eugene W. Myers, and David J. Lipman. Basic local alignment search tool. *Journal of Molecular Biology*, 215:403–410, 1990.

- [31] Michael Blazanin. *gcplyr*: an r package for microbial growth curve data analysis. *BMC bioinformatics*, 25(1):232, 2024.
- [32] R Core Team. *R: A Language and Environment for Statistical Computing*. R Foundation for Statistical Computing, Vienna, Austria, 2023.
- [33] Robert May and Angela R McLean. *Theoretical ecology: principles and applications*. OUP Oxford, 2007.

# S1 Mathematical models of competition

We used mathematical modeling to understand the impact of a deteriorating environment on the competition between two or more species. The generalized Lotka-Volterra model is a powerful framework to describe such ecological competition, summarizing complex biological processes (e.g. resource competition, competition for space or toxin production) into either self-inhibition ( $a_{ii}$ ) or the net effect of species  $N_j$  on the growth of  $N_i$  ( $a_{ij}$ ). In serial dilution experiments in the laboratory, as well as most natural environments, species will also be removed (or die) at a constant rate  $\delta$ .

This yields the general model equations governing the population size  $N_i$  of species  $i$ :

$$\frac{dN_i}{dt} = r_i(s)N_i \cdot (1 - \sum_{j \in 1 \dots M} a_{ij}N_j) - \delta N_i, \quad (2)$$

where  $r_i(s)$  denotes the growth rate in environment  $s$ , and the self-inhibition terms are  $a_{ii} > 0$ . The interaction terms between both species  $a_{ij}$  can take any real number.

## S1.1 Pairwise Model

To study the dynamics of these equations in more detail, we first focus on the case with two species ( $N_1, N_2$ ).

$$\begin{aligned} \frac{dN_1}{dt} &= r_1 N_1 \cdot (1 - a_{11}N_1 - a_{12}N_2) - \delta N_1 \\ \frac{dN_2}{dt} &= r_2 N_2 \cdot (1 - a_{22}N_2 - a_{21}N_1) - \delta N_2 \end{aligned} \quad (3)$$

The classical form of 2-species LV equations can be obtained by integrating the dilution rate into new effective parameters [6, 4, 5]:

$$\tilde{a}_{ij} = a_{ij} \frac{1 - \frac{\delta}{r_j}}{1 - \frac{\delta}{r_i}}, \quad \tilde{r}_i = r_i - \delta, \quad \tilde{N}_i = N_i \frac{1}{1 - \frac{\delta}{r_i}}. \quad (4)$$

For the first ODE this yields:

$$\begin{aligned} \frac{d\tilde{N}_1}{dt} &= \frac{1}{1 - \frac{\delta}{r_1}} \frac{dN_1}{dt} \\ &= \frac{1}{1 - \frac{\delta}{r_1}} \cdot r_1 \left(1 - \frac{\delta}{r_1}\right) \tilde{N}_1 \cdot \left(1 - \frac{\delta}{r_1} - \tilde{a}_{11} \left(1 - \frac{\delta}{r_1}\right) \tilde{N}_1 - \tilde{a}_{12} \frac{1 - \frac{\delta}{r_1}}{1 - \frac{\delta}{r_2}} \left(1 - \frac{\delta}{r_2}\right) \tilde{N}_2\right) \\ &= r_1 \left(1 - \frac{\delta}{r_1}\right) \tilde{N}_1 \cdot \left(1 - \tilde{a}_{11} \tilde{N}_1 - \tilde{a}_{12} \tilde{N}_2\right) \\ &= \tilde{r}_1 \tilde{N}_1 \cdot \left(1 - \tilde{a}_{11} \tilde{N}_1 - \tilde{a}_{12} \tilde{N}_2\right). \end{aligned}$$

So we recover the new system of equations:

$$\begin{aligned} \frac{d\tilde{N}_1}{dt} &= \tilde{r}_1 \tilde{N}_1 \cdot \left(1 - \tilde{a}_{11} \tilde{N}_1 - \tilde{a}_{12} \tilde{N}_2\right) \\ \frac{d\tilde{N}_2}{dt} &= \tilde{r}_2 \tilde{N}_2 \cdot \left(1 - \tilde{a}_{22} \tilde{N}_2 - \tilde{a}_{21} \tilde{N}_1\right). \end{aligned} \quad (5)$$

**Steady state outcomes** To obtain an analytical expression for the steady-state outcome of the competition between  $N_1$  and  $N_2$ , we solve ODE 3 at  $\frac{dN_1}{dt} = 0 = \frac{dN_2}{dt}$ . We find the following four outcomes:

$$N_1 = 0, N_2 = 0 \quad (6)$$

$$N_1 = 0, N_2 = \frac{r_2 - \delta}{a_{22}r_2} \quad (7)$$

$$N_1 = \frac{r_1 - \delta}{a_{11}r_1}, N_2 = 0 \quad (8)$$

$$N_1 = -\frac{a_{12}\delta r_1 - a_{22}\delta r_2 - a_{12}r_1r_2 + a_{22}r_1r_2}{(a_{12}a_{21} - a_{11}a_{22})r_1r_2}, \\ N_2 = -\frac{-a_{11}\delta r_1 + a_{21}\delta r_2 + a_{11}r_1r_2 - a_{21}r_1r_2}{(a_{12}a_{21} - a_{11}a_{22})r_1r_2}. \quad (9)$$

This is equivalent to:

$$\tilde{N}_1 = 0, \tilde{N}_2 = 0 \quad (10)$$

$$\tilde{N}_1 = 0, \tilde{N}_2 = \frac{1}{\tilde{a}_{22}} \quad (11)$$

$$\tilde{N}_1 = \frac{1}{\tilde{a}_{11}}, \tilde{N}_2 = 0 \quad (12)$$

$$\tilde{N}_1 = \frac{\tilde{a}_{12} - \tilde{a}_{22}}{\tilde{a}_{12}\tilde{a}_{21} - \tilde{a}_{11}\tilde{a}_{22}}, \tilde{N}_2 = \frac{\tilde{a}_{21} - \tilde{a}_{11}}{\tilde{a}_{12}\tilde{a}_{21} - \tilde{a}_{11}\tilde{a}_{22}}. \quad (13)$$

**Coexistence, bistability or exclusion** The fourth steady state allows positive species abundances when  $\tilde{a}_{12} > \tilde{a}_{22}$  and  $\tilde{a}_{21} > \tilde{a}_{11}$  or  $\tilde{a}_{12} < \tilde{a}_{22}$  and  $\tilde{a}_{21} < \tilde{a}_{11}$ . It is easy to see that the first set of constraints yields a bistable system, where species 1 more strongly inhibits species 2 than species 1 inhibits itself and vice versa, while the second set of constraints yields coexistence [33].

As such we find the following conditions for the canonical version of the LV model with effective parameters  $\tilde{a}_{12}, \tilde{a}_{21}$ :

$$\text{Coexistence : } \frac{\tilde{a}_{12}}{\tilde{a}_{22}} < 1, \frac{\tilde{a}_{21}}{\tilde{a}_{11}} < 1 \quad (14)$$

$$N_1 \text{ wins : } \frac{\tilde{a}_{12}}{\tilde{a}_{22}} < 1, \frac{\tilde{a}_{21}}{\tilde{a}_{11}} > 1 \quad (15)$$

$$N_2 \text{ wins : } \frac{\tilde{a}_{12}}{\tilde{a}_{22}} > 1, \frac{\tilde{a}_{21}}{\tilde{a}_{11}} < 1 \quad (16)$$

$$\text{Bistability : } \frac{\tilde{a}_{12}}{\tilde{a}_{22}} > 1, \frac{\tilde{a}_{21}}{\tilde{a}_{11}} > 1 \quad (17)$$

And for the corresponding equations with the full parameters:

$$\text{Coexistence : } \frac{a_{12}}{a_{22}} \frac{r_1r_2 - \delta r_1}{r_1r_2 - \delta r_2} < 1 \quad \frac{a_{21}}{a_{11}} \frac{r_1r_2 - \delta r_2}{r_1r_2 - \delta r_1} < 1 \quad (18)$$

$$N_1 \text{ wins : } \frac{a_{12}}{a_{22}} \frac{r_1r_2 - \delta r_1}{r_1r_2 - \delta r_2} < 1 \quad \frac{a_{21}}{a_{11}} \frac{r_1r_2 - \delta r_2}{r_1r_2 - \delta r_1} > 1 \quad (19)$$

$$N_2 \text{ wins : } \frac{a_{12}}{a_{22}} \frac{r_1r_2 - \delta r_1}{r_1r_2 - \delta r_2} > 1 \quad \frac{a_{21}}{a_{11}} \frac{r_1r_2 - \delta r_2}{r_1r_2 - \delta r_1} < 1 \quad (20)$$

$$\text{Bistability : } \frac{a_{12}}{a_{22}} \frac{r_1r_2 - \delta r_1}{r_1r_2 - \delta r_2} > 1 \quad \frac{a_{21}}{a_{11}} \frac{r_1r_2 - \delta r_2}{r_1r_2 - \delta r_1} > 1 \quad (21)$$

In the coexistence state (equations 9 or 13) the ratio of  $N_1/N_2$  is given by:

$$\frac{N_1}{N_2} = \frac{a_{22}\delta r_2 - r_1(a_{12}\delta + (a_{22} - a_{12})r_2)}{a_{11}\delta r_1 - r_2(a_{21}\delta + (a_{11} - a_{21})r_1)} \quad (22)$$

Or equivalently:

$$\frac{\tilde{N}_1}{\tilde{N}_2} = \frac{\tilde{a}_{22} - \tilde{a}_{12}}{\tilde{a}_{11} - \tilde{a}_{21}} \quad (23)$$

**Changing salinity** The previous results hold generically, for any two species whose competition can be described in a Lotka-Volterra framework with dilution (eq. 3). However, now we can ask how these steady state outcomes change as the environment changes. We assume that the interspecies interactions ( $a_{ij}$ ) and carrying capacities ( $1/a_{ii}$ ) do not change with salinity. Then we see that for the three nontrivial steady state outcomes (eq. 9), the final steady state abundance of each population is determined by the functional relationship between growth rate and salinity.

For simplicity, we assume specific scenarios:

- Parallel growth curves: the two species exhibit different maximal growth rates  $r_1^{max}, r_2^{max}$ , which decrease linearly at the same rate  $b$ :  

$$r_i(s) = r_i^{max} - b \cdot s .$$
- Converging growth curves: the two species exhibit different maximal growth rates  $r_1^{max}, r_2^{max}$ , which decrease linearly to the same point  $s^{max}$ :  

$$r_i(s) = r_i^{max} - \frac{r_i^{max}}{s^{max}} s .$$
- Diverging growth curves: the two species exhibit the same maximal growth rate  $r^{max}$ , which decrease linearly at different rates  $b_1, b_2$ :  

$$r_i(s) = r^{max} - b_i \cdot s .$$

In each case, we want to know how the ratio between both species  $N_1/N_2$  changes with increasing salinity. To do so, we calculate the derivative of eq. 22 with respect to  $s$  upon substitution of these different linear functions for  $r_1(s), r_2(s)$ .

Parallel growth curves:

$$\frac{d}{ds} \frac{N_1}{N_2} = \frac{(a_{12}a_{21} - a_{11}a_{22})\delta \cdot b \cdot (r_1^{max} - r_2^{max})(\delta - r_1(s) - r_2(s))}{(a_{21}r_2(s)(\delta - r_1(s)) - a_{11}r_1(s)(\delta - r_2(s)))^2} \quad (24)$$

Under the conditions that yield coexistence, i.e.  $a_{12}a_{21} < a_{11}a_{22}$ , and assuming that  $r_1 > r_2$  and  $\delta < r_1 + r_2$ , we find that  $\frac{d}{ds} \frac{N_1}{N_2} > 0$ . The proportion of the faster growing species increases with increasing salinity.

We can perform the same analysis for converging growth curves:

$$\frac{d}{ds} \frac{N_1}{N_2} = \frac{-(a_{12}a_{21} - a_{11}a_{22})\delta r_1^{max} r_2^{max} (r_1^{max} - r_2^{max})}{s^{max} (a_{21}r_2^{max}(\delta - r_1(s)) - a_{11}r_1^{max}(\delta - r_2(s)))^2} \quad (25)$$

or diverging growth curves:

$$\frac{d}{ds} \frac{N_1}{N_2} = \frac{(a_{12}a_{21} - a_{11}a_{22})\delta(b_1 - b_2)((r^{max})^2 - r^{max}\delta - b_1 b_2 s^2)}{(a_{21}r_2(s)(\delta - r_1(s)) - a_{11}r_1(s)(\delta - r_2(s)))^2} \quad (26)$$

Across all scenarios a high dilution rate  $\delta$  contributes to a strong effect of salinity on the proportion of the faster growing species.

## S2 Supplementary Figures

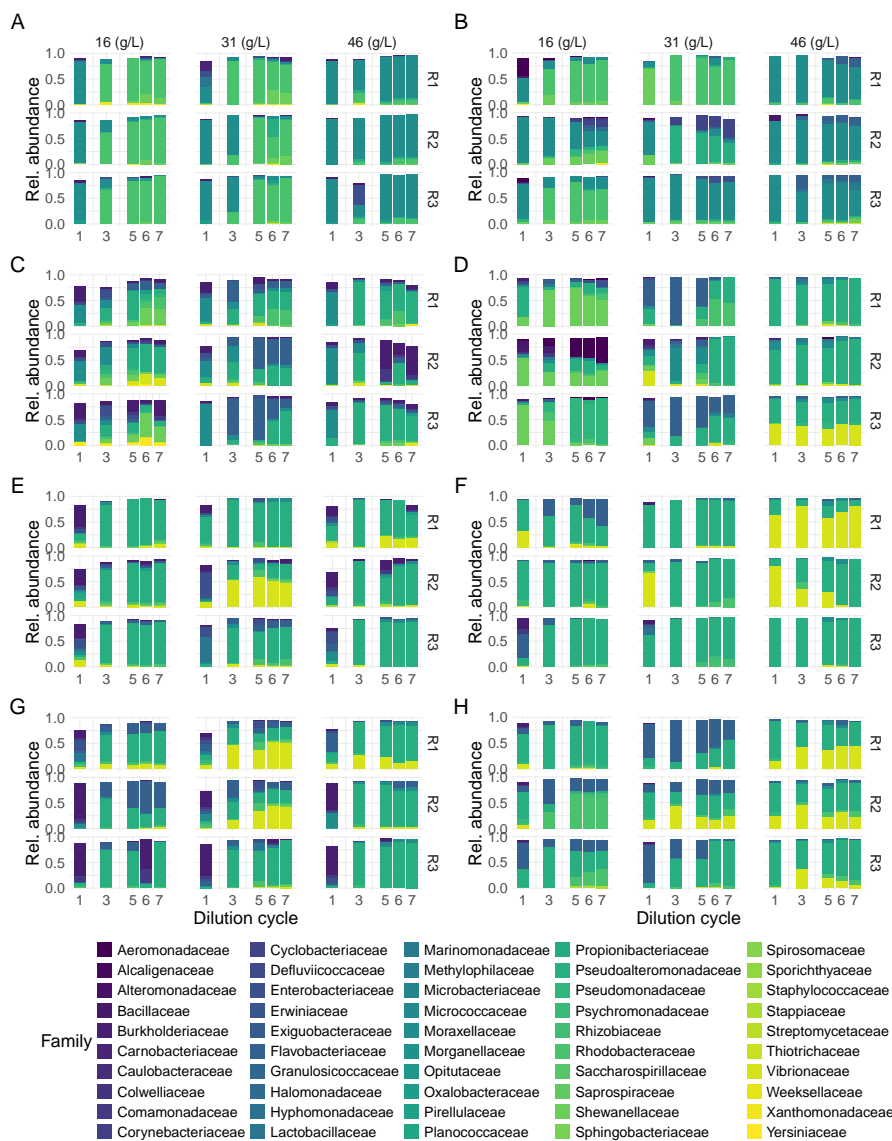


**Figure S1: Community composition over 7 growth-dilution cycles.** Communities are separated by the propagation temperature (columns) and the source community (rows): A) Brackish 15°C, B) Brackish 20°C, C) Estuary 15°C, D) Estuary 20°C, E) Marine 1 15°C, F) Marine 1 20 °C, G) Marine 2 15°C, H) Marine 2 20 °C. Three replicate communities (R1-3) were propagated for each condition. ASVs are colored by taxonomic family, and only ASVs at greater than 1% relative abundance are depicted.

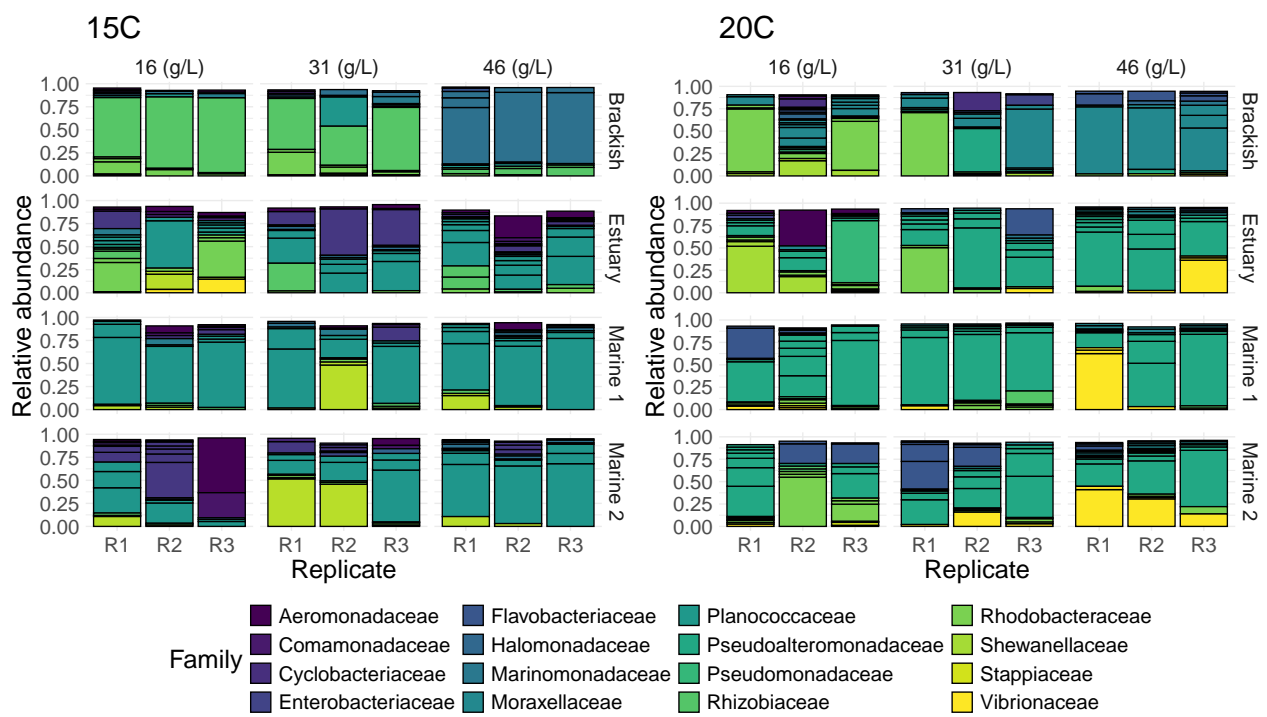


**Figure S2: Community composition after cycle 6.** Communities are separated by the temperature (left and right panel; 15°C and 20°C) and salinity (columns within each panel; 16, 31, or 46 g/L) they were propagated at, as well as the source community (rows within each panel; Brackish, Estuary, Marine 1/2). Three replicate communities (R1-3) were propagated for each condition. ASVs are colored by taxonomic family, and only ASVs at greater than 1% relative abundance are depicted.

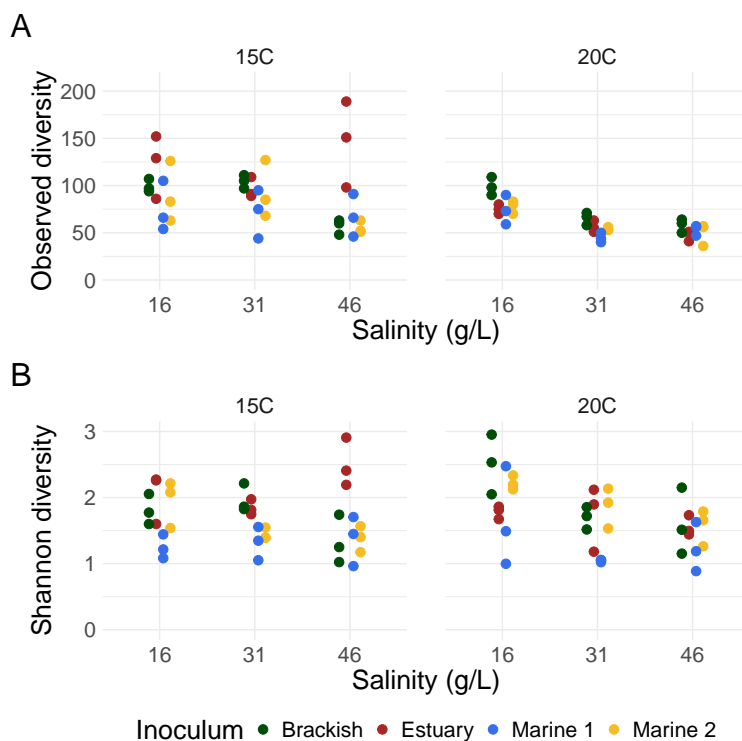


**Figure S3: Diversity of the communities after 6 cycles of passaging.** A) Observed and B) Shannon diversity of the propagated communities after 6 cycles. Diversity metrics are based on the 16S community sequencing data, assuming each ASV is a unique species. Colors represent the different starting communities.

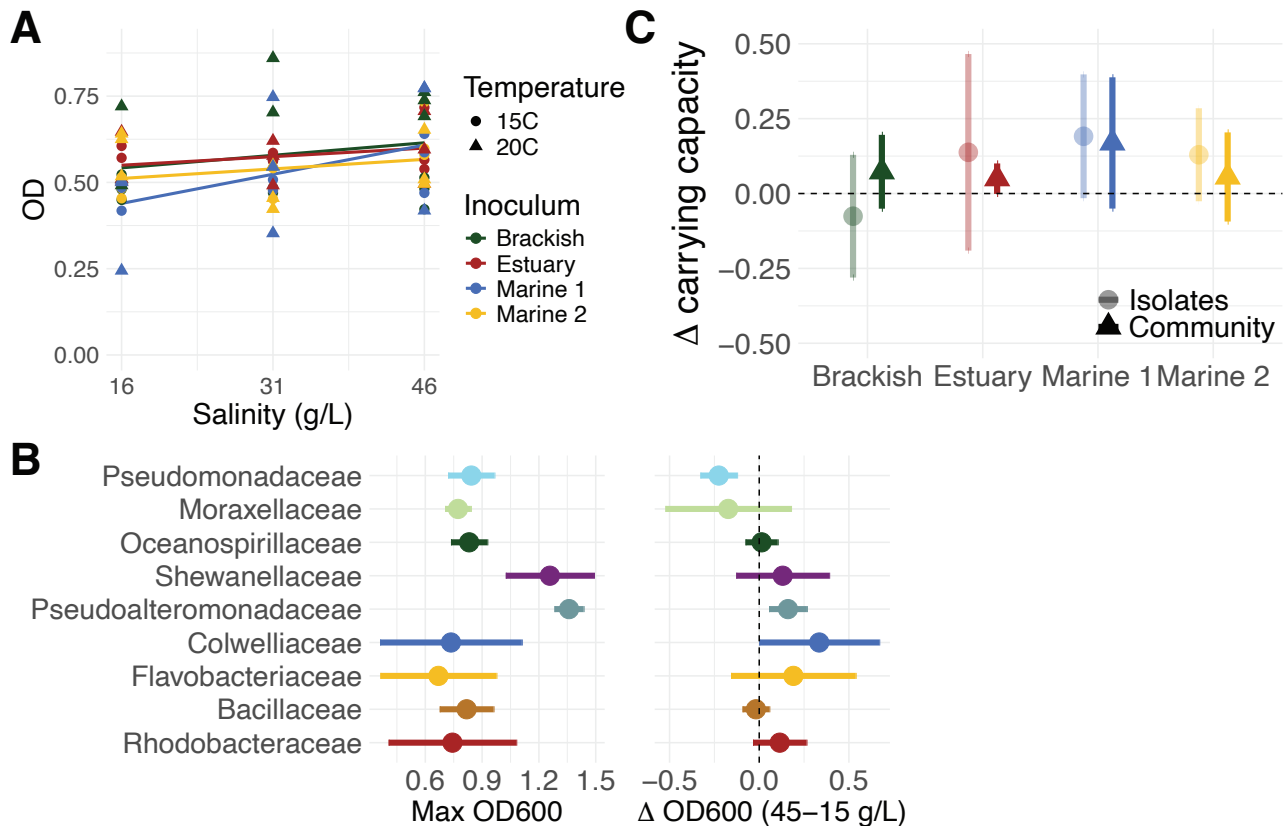


**Figure S4: The carrying capacities of isolates and communities are robust to an increase in salinity. A)** The OD600 of each community at the end of the serial dilution experiment (C6). **B)** Summary statistics of isolate carrying capacities, grouped by family. Shown are the maximum carrying capacity (approximated by max OD600 in monoculture) obtained across all salinities, as well as the change in carrying capacity between growth at 45 and 15 g/L. **C)** The mean change in carrying capacity between 15 and 45 g/L, for communities (dark triangles) and isolates (light circles).

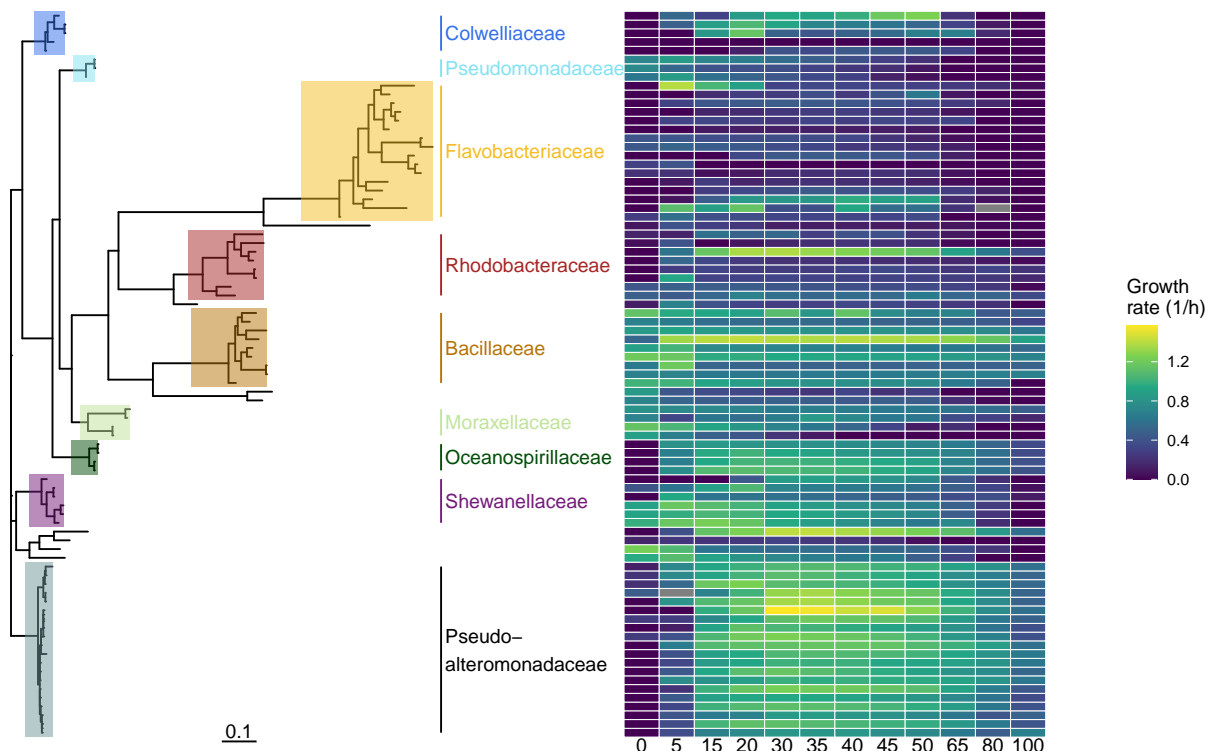


**Figure S5: Maximum likelihood phylogenetic tree of the isolate 16S gene sequence, with the measured growth rates as a function of salinity (g/L).** The tree is rooted at an arbitrary point to highlight major clades. Families with at least 3 isolates are highlighted in colors corresponding to Fig. 1C.

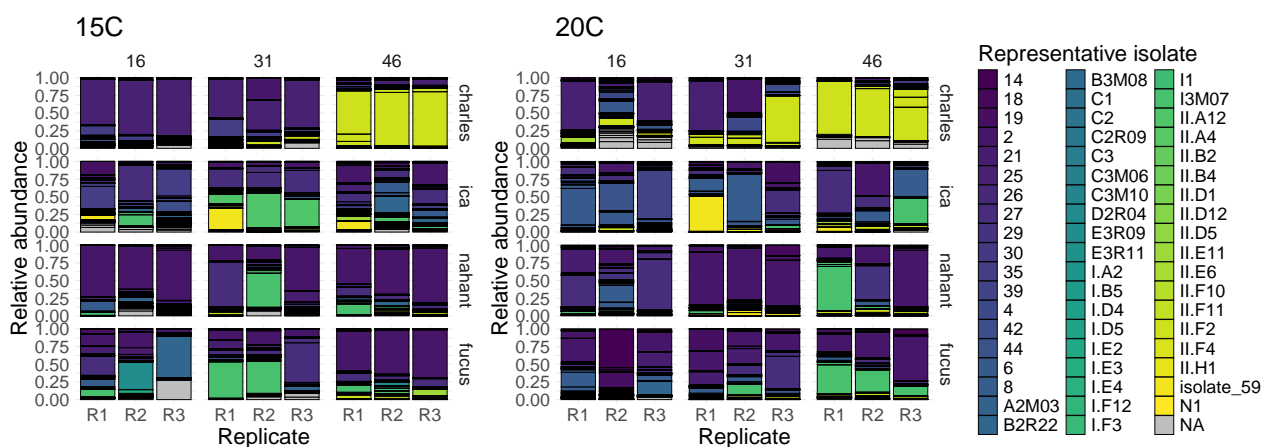


**Figure S6: Our isolates cover the diversity observed at the end of the serial dilution experiment.** An isolate is considered a match to an ASV if the 16S sequences are > 97% similar. If more than one isolate match the same ASV equally well, their growth rates are averaged. Columns correspond to different salinities (16, 31, or 46 g/L), subdivided into three replicates (R1, R2, R3). Rows correspond to different inoculum communities.

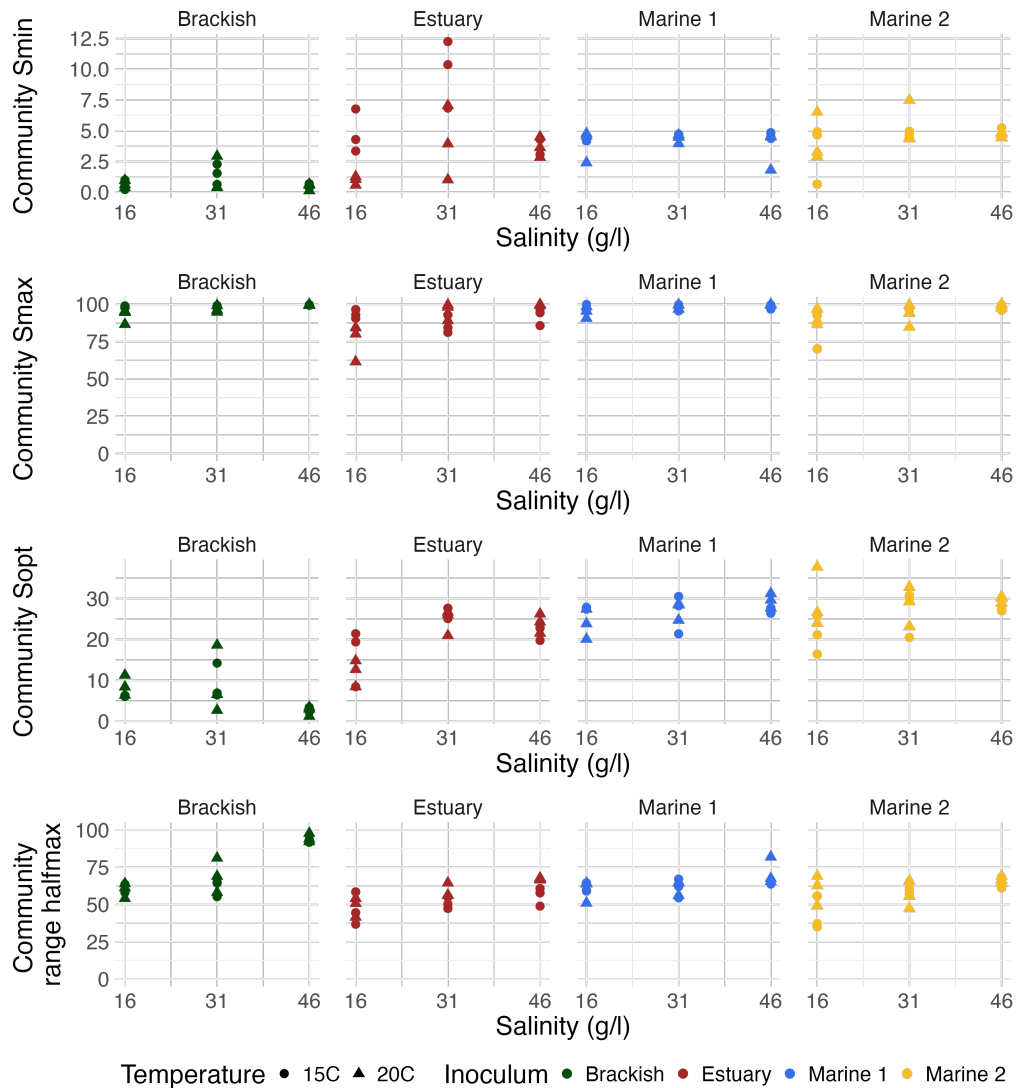


**Figure S7: Community averages of four parameters of the salinity performance curve.**  
 We mapped ASVs to isolates and for each isolate extracted the minimal salinity at which the isolate grows ( $s_{min}$ ), the maximum salinity at which it grows ( $s_{max}$ ), the salinity at which maximal growth is reached ( $s_{opt}$ ) and the width of the salinity range for which the isolate realizes at least half its maximal growth rate. Depicted are the average of these quantities for each community, weighted by the relative abundance of each ASV.

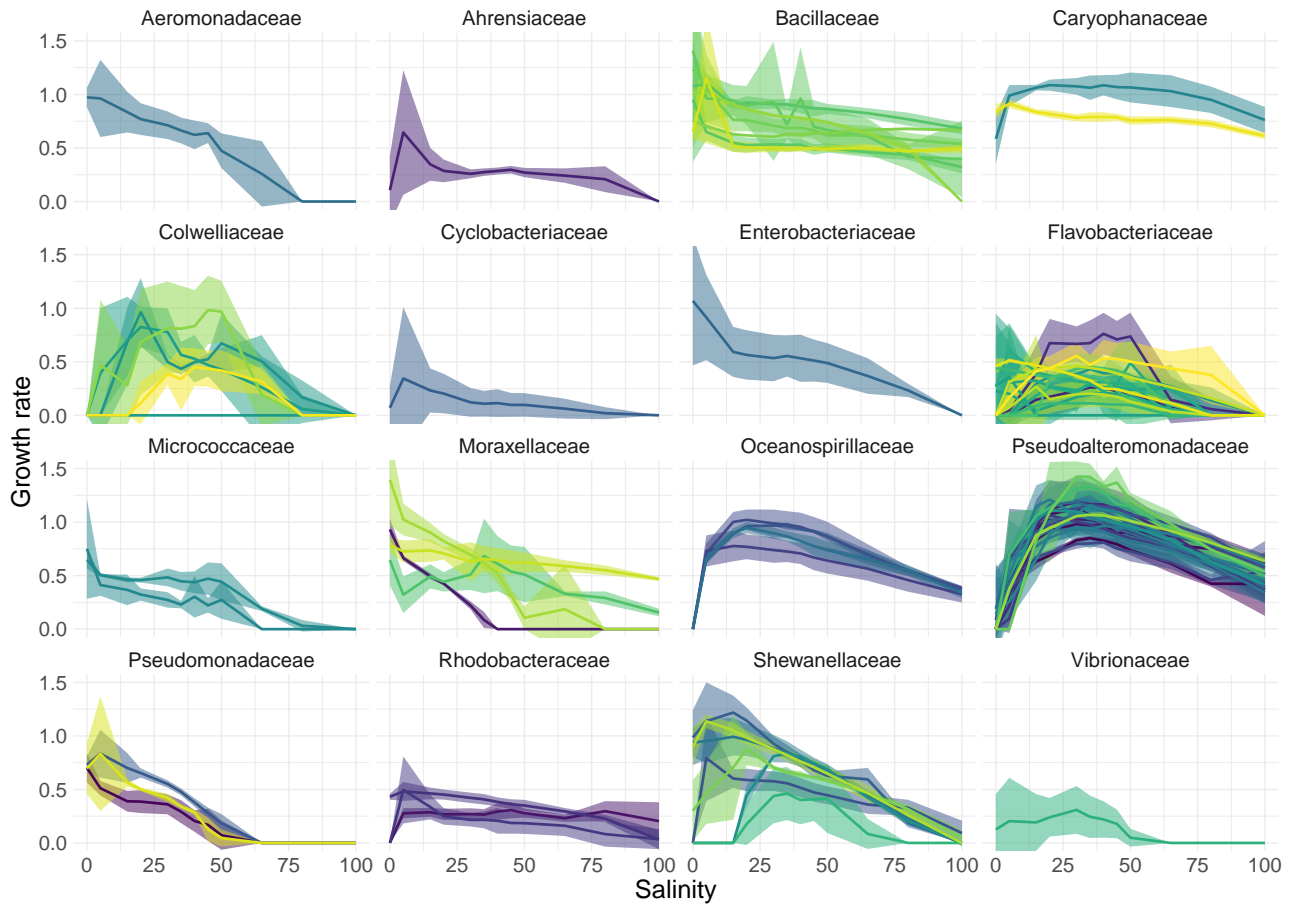


**Figure S8: Salinity performance curves for all isolates in our dataset, grouped by family.** Maximum growth rate was measured at 12 different salinities (0, 5, 15, 20, 30, 35, 40, 45, 50, 65, 80, 100 g/L). Isolates are assigned different colors, solid lines indicate the mean across all measurements for an isolate ( $n \geq 3$ ) and ribbons indicate mean  $\pm$  sd.

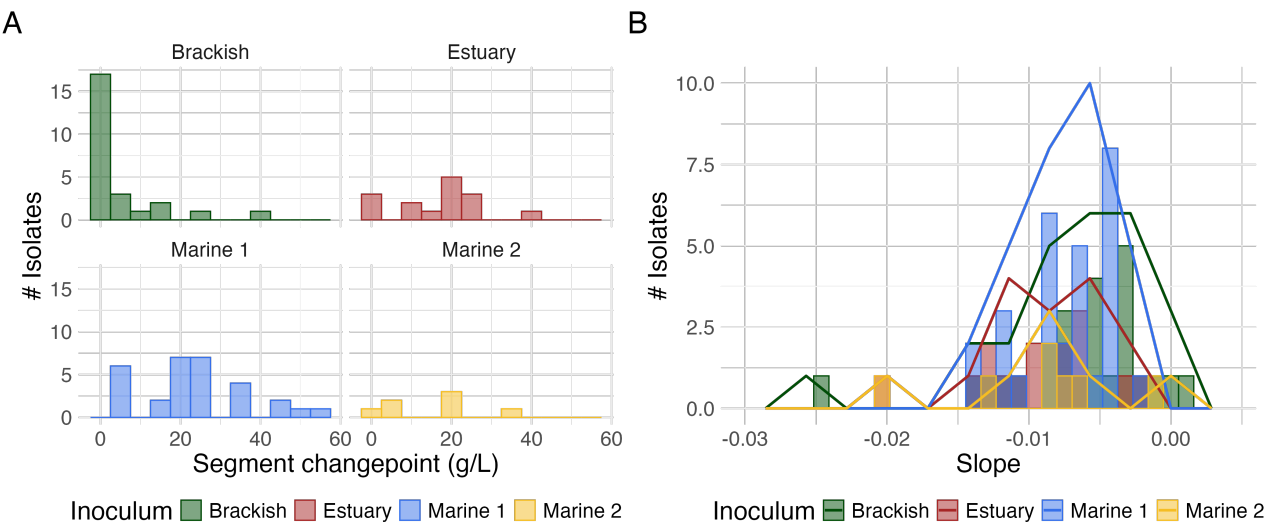


**Figure S9: Growth parameters of marine species as fitted with 2-segment models.** **A** Salinity at which the maximal growth rate is reached. This corresponds to either the breakpoint of the 2-segment model or a salinity of 0 g/L if both the first and second slope were negative. **B** The inferred slope of growth rate (1/h) as a function of salinity (g/L) after the optimum.

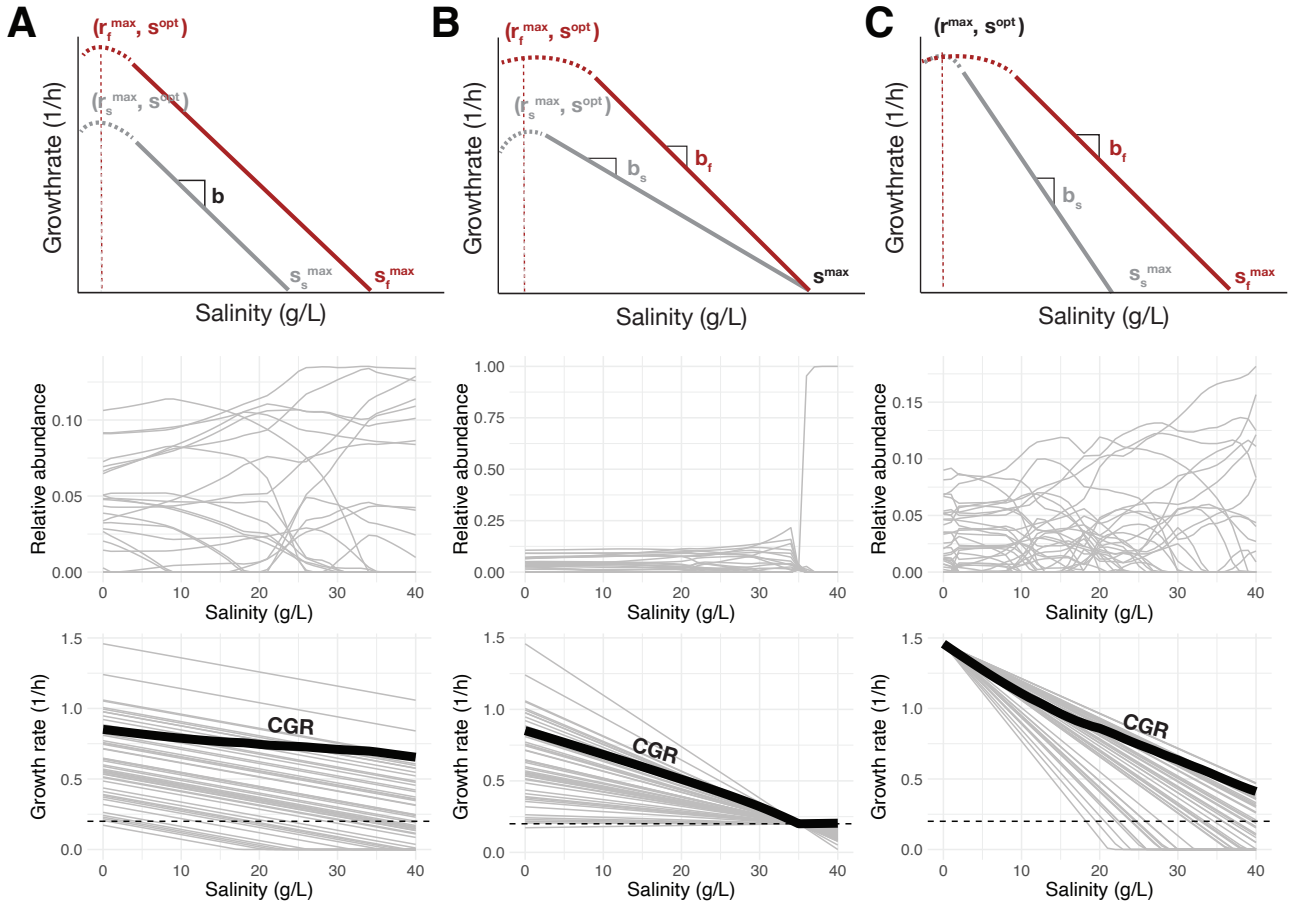


**Figure S10: Simulations show that the proportion of faster growing species robustly increases, independent of the distribution of growth rates as a function of salinity.** We compare three different scenarios: column A corresponds to a community with parallel declines in growth rate (the scenario depicted in main text Fig. 2); B corresponds to a scenario with different starting growth rate and slopes, but the same maximal salinity conducive of growth; C corresponds to a scenario with the same starting growth rate, but different slopes and different maximal salinities. In the growth rate panels (bottom row), the thick black line indicates the community growth rate (CGR), the abundance weighted mean of the realized growth rates of all species in the community. The dashed horizontal line indicates the strength of the removal rate  $\delta$ .

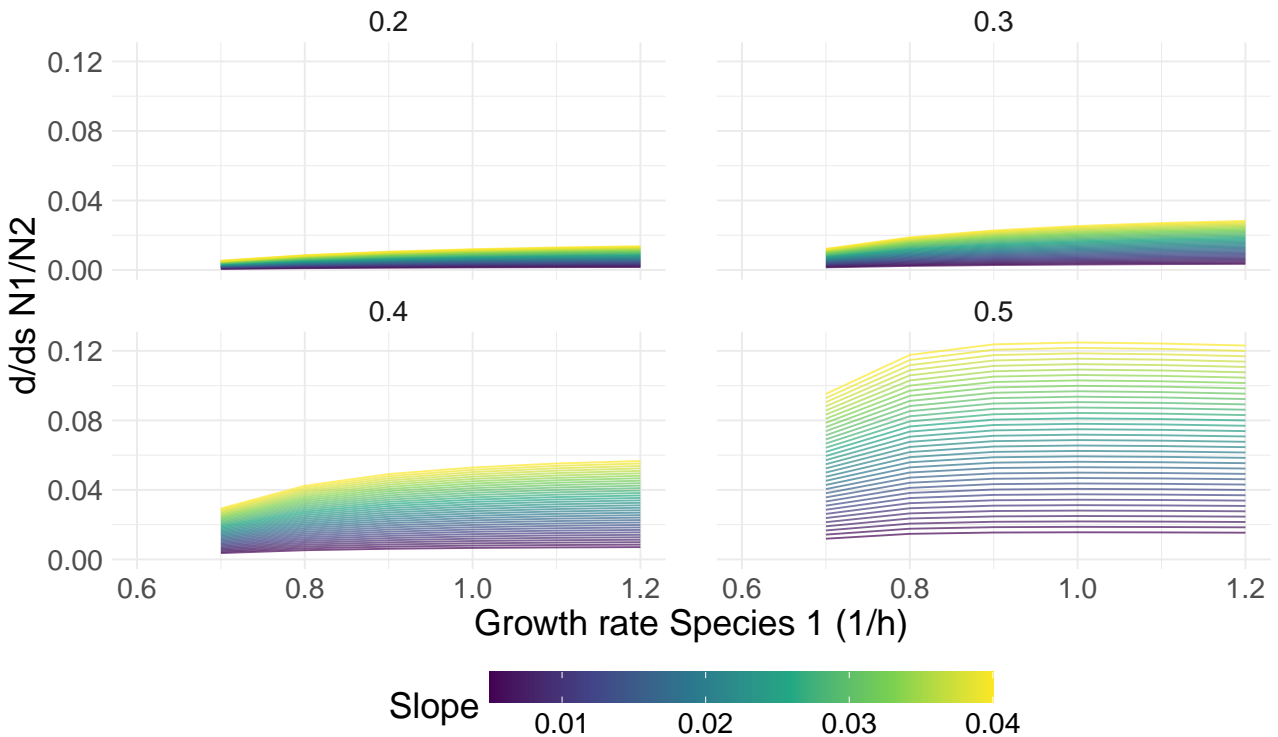


**Figure S11: Analytical results of equation 24 for different growth rates, mortality rates (facets) and slopes of growth as a function of salinity (colors).** Derivatives were calculated at the optimal salinity (here  $S_{opt} = 0$ ), assuming species 2 has a growth rate  $r_s = 0.6$ .

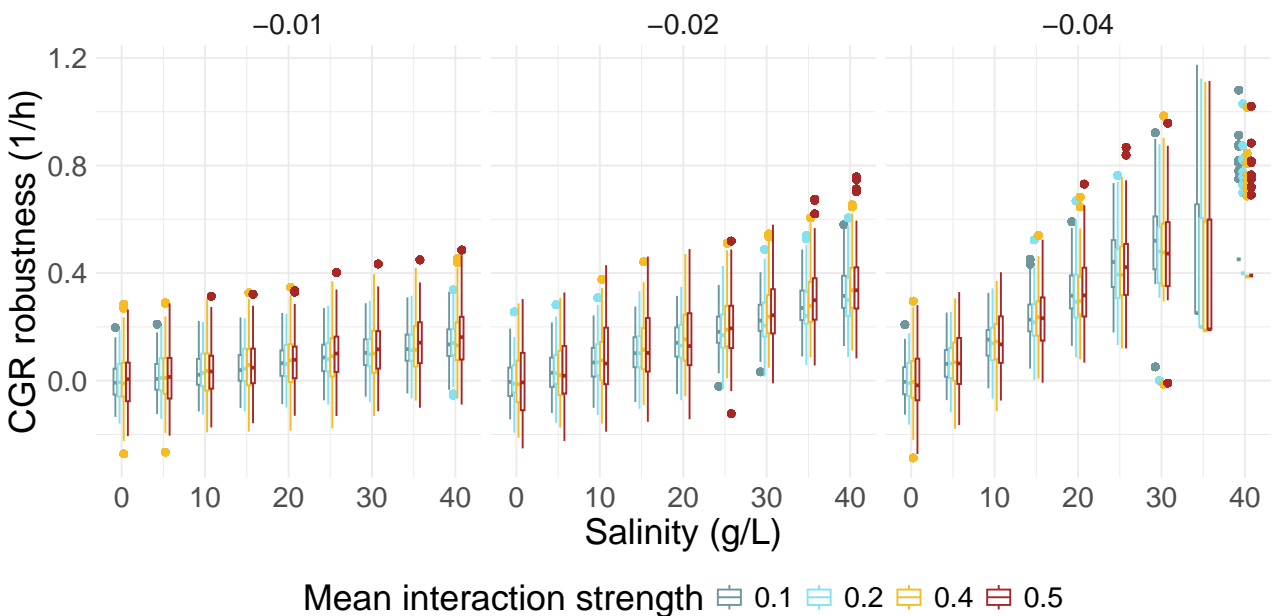


**Figure S12: Slope of the growth rate, but not interaction strength, affect the robustness of the community growth rate (CGR) as a function of salinity.** Robustness was calculated as the realized CGR - the average decline in species growth at that salinity. In these simulations, the robustness in the CGR exactly mirrors the shift in the community composition index (CCI). Columns indicate different slopes of the growth rate as a function of salinity, and colors different values of the mean interaction strength  $\alpha$ . Each boxplot summarizes 50 simulations of 50-species communities.

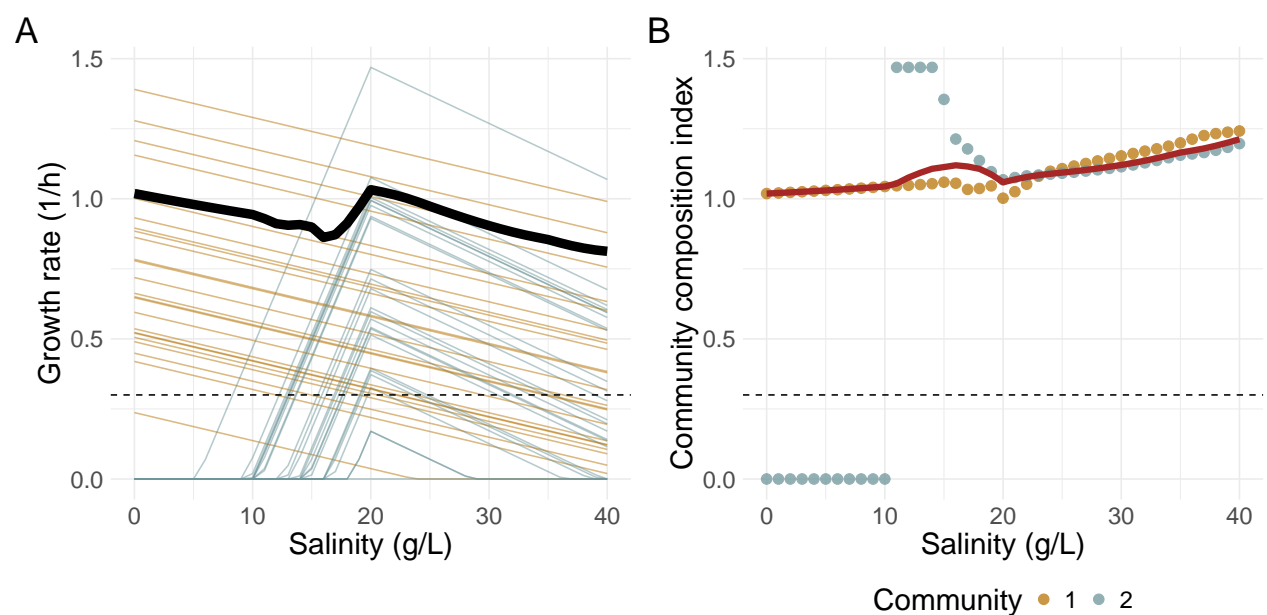


**Figure S13: Modeling suggests that the community growth rate remains robust when isolates with two different optimal salinities are mixed.** Simulations were initiated with a total of 50 isolates, half of which had  $s^{opt} = 0$  (Community 1, yellow) and the other half  $s^{opt} = 20$  (Community 2, blue). Community growth rate was robust across a broad range (black line), and the community composition index (red line) increased.

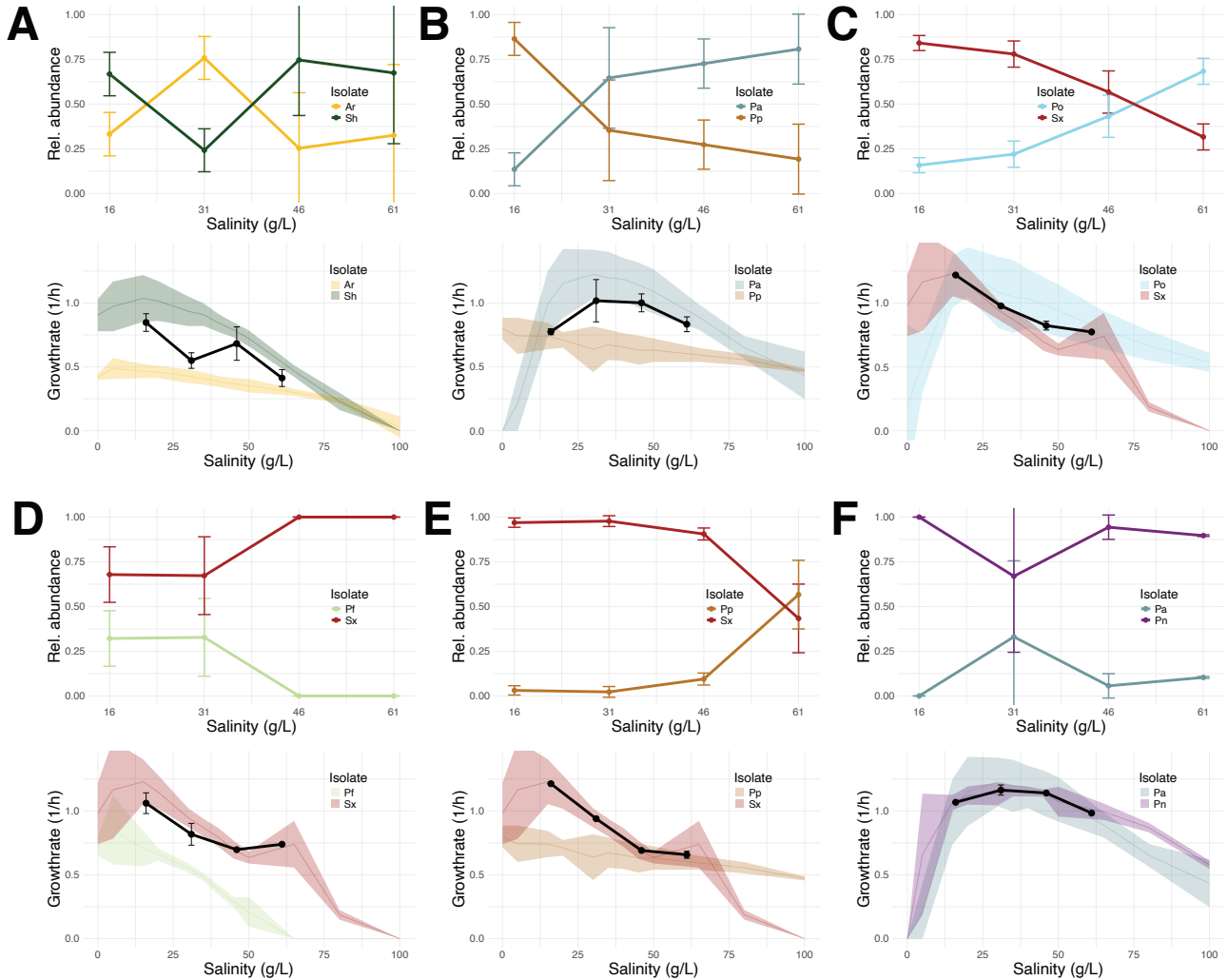


**Figure S14: In pairwise co-culture, higher salinity favors the faster growing species.**

A) Salinity performance curves for the two species in each pair (ribbons show mean  $\pm$  sd across  $n \geq 3$  replicates). The black line indicates the CGR of the pairs after 14 days of propagation at 16, 31, 46, 61 g/L salinity. B) Relative abundance of both isolates in a pair after propagation at 4 salinities (16, 31, 46, 61 g/L) for 14 days. Mean and sd across three biological replicates at three different initial ratios (5:95, 50:50, 95:5). Abbreviations indicate: *Pseudoalteromonas arctica* (*Pa*), *Shewanella xiamensis* (*Sx*), *Shewanella* sp. (*Sh*), *Albirhodobacter* sp. (*Ar*), *Pseudoalteromonas ostrae* (*Po*), *Pseudoalteromonas nitrificiens* (*Pn*), *Pseudomonas fragi* (*Pf*), and *Psychrobacter piscatorii* (*Pp*).

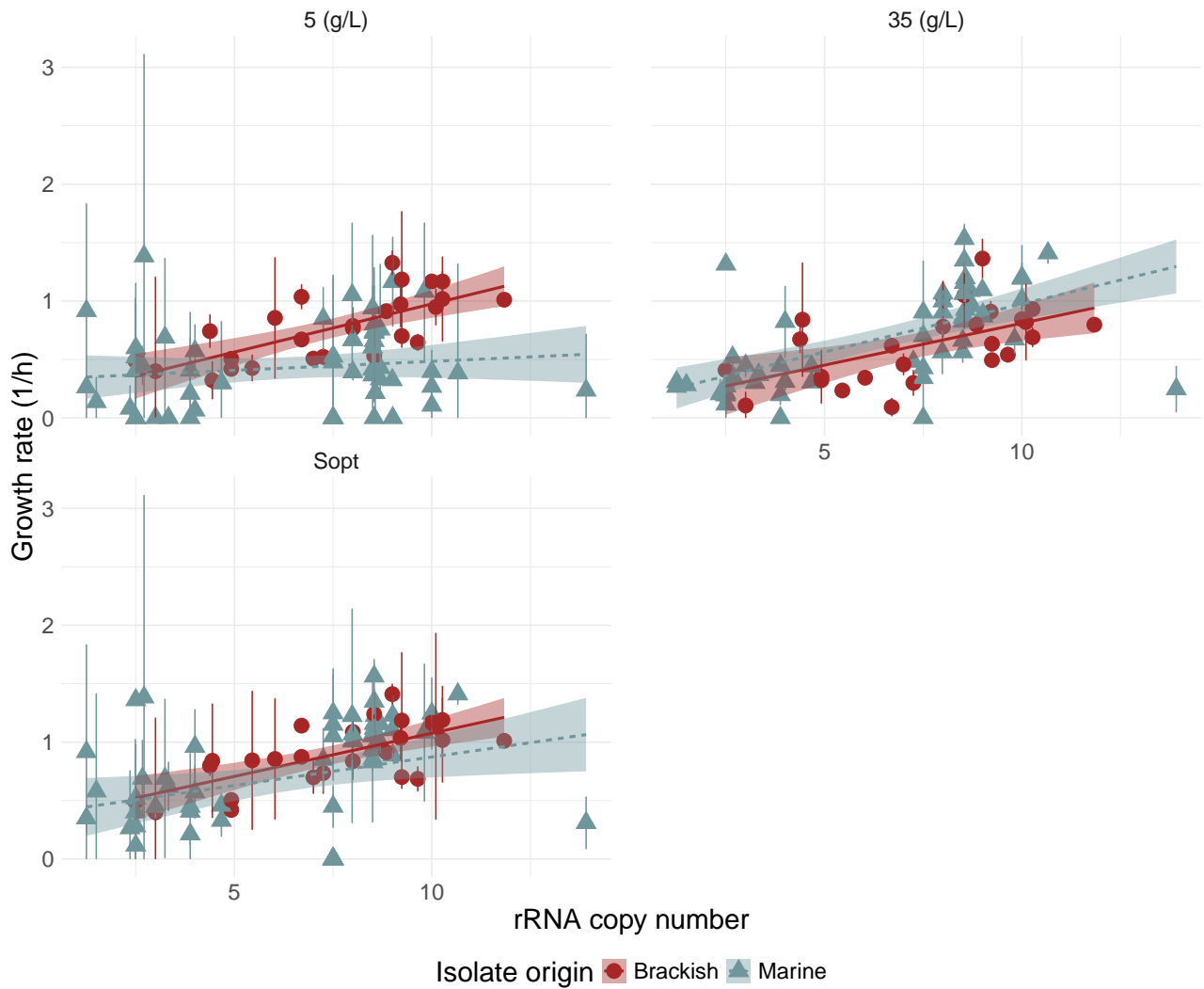


**Figure S15: Growth rate of an isolate at its isolation salinity correlates strongly with its predicted 16S rRNA copy number.** Isolates are colored by their isolation location. For the purpose of this analysis isolates from the Estuary sampling location (30 g/L) were grouped with the Marine isolates (35 g/L). The third panel, Sopt, associates each isolate with its maximal growth rate (at salinity  $s_{opt}$ ).